AGU PUBLICATIONS

Paleoceanography

RESEARCH ARTICLE
10.1002/2014PA002707

**Key Points:**
- Northern Hemisphere signal in Southern Ocean Nd isotopes related to NADW
- Role for precessional forcing of ocean circulation during glacial inception
- Ocean circulation and carbon storage decoupled within glacial periods

**Supporting Information:**
- Tables S1–S6

**Correspondence to:**
D. J. Wilson,
david.wilson1@imperial.ac.uk

**Citation:**
Wilson, D. J., A. M. Piotrowski, A. Galy, and V. K. Banakar (2015), Interhemispheric controls on deep ocean circulation and carbon chemistry during the last two glacial cycles, *Paleoceanography*, *30*, 621–641, doi:10.1002/2014PA002707.

Received 5 AUG 2014
Accepted 28 APR 2015
Accepted article online 2 MAY 2015
Published online 6 JUN 2015



# Interhemispheric controls on deep ocean circulation and carbon chemistry during the last two glacial cycles

**David J. Wilson[1,2], Alexander M. Piotrowski[1], Albert Galy[1,3], and Virupaxa K. Banakar[4]**

[1]Godwin Laboratory for Palaeoclimate Research, Department of Earth Sciences, University of Cambridge, Cambridge, UK, [2]Department of Earth Science and Engineering, Imperial College London, London, UK, [3]CRPG, Université de Lorraine, CNRS, Vandoeuvre-lès-Nancy, France, [4]National Institute of Oceanography, Dona Paula, India

**Abstract** Changes in ocean circulation structure, together with biological cycling, have been proposed for trapping carbon in the deep ocean during glacial periods of the Late Pleistocene, but uncertainty remains in the nature and timing of deep ocean circulation changes through glacial cycles. In this study, we use neodymium (Nd) and carbon isotopes from a deep Indian Ocean sediment core to reconstruct water mass mixing and carbon cycling in Circumpolar Deep Water over the past 250 thousand years, a period encompassing two full glacial cycles and including a range of orbital forcing. Building on recent studies, we use reductive sediment leaching supported by measurements on isolated phases (foraminifera and fish teeth) in order to obtain a robust seawater Nd isotope reconstruction. Neodymium isotopes record a changing North Atlantic Deep Water (NADW) component in the deep Indian Ocean that bears a striking resemblance to Northern Hemisphere climate records. In particular, we identify both an approximately in-phase link to Northern Hemisphere summer insolation in the precession band and a longer-term reduction of NADW contributions over the course of glacial cycles. The orbital timescale changes may record the influence of insolation forcing, for example via NADW temperature and/or Antarctic sea ice extent, on deep stratification and mixing in the Southern Ocean, leading to isolation of the global deep oceans from an NADW source during times of low Northern Hemisphere summer insolation. That evidence could support an active role for changing deep ocean circulation in carbon storage during glacial inceptions. However, mid-depth water mass mixing and deep ocean carbon storage were largely decoupled within glacial periods, and a return to an interglacial-like circulation state during marine isotope stage (MIS) 6.5 was accompanied by only minor changes in atmospheric $CO_2$. Although a gradual reduction of NADW export through glacial periods may have produced slow climate feedbacks linked to the growth of Northern Hemisphere ice sheets, carbon cycling in the glacial ocean was instead more strongly linked to Southern Ocean processes.

## 1. Introduction

Deep ocean circulation changes are often invoked in explanations of glacial-interglacial climate change because of the ocean's role in regulating interhemispheric heat transport and global carbon storage [*Broecker and Denton*, 1989; *Toggweiler*, 1999; *Toggweiler et al*., 2006; *Sigman et al*., 2010]. In particular, a more isolated deep ocean during glacial periods may have stored more dissolved inorganic carbon, contributing significantly to the glacial reduction in atmospheric $CO_2$. The subsequent release of this deeply sequestered $CO_2$ was a key component in the sequence of changes that occurred during deglaciation [*Anderson et al*., 2009; *Skinner et al*., 2010; *Yu et al*., 2010; *Burke and Robinson*, 2012]. In contrast to those changes during deglaciation, the processes involved in glacial inception remain poorly understood. More generally, it remains an open question whether ocean circulation actively forced climate change or was limited to an amplifying (feedback) process. This uncertainty limits our understanding of the mechanisms by which the Earth system has amplified relatively small changes in orbital forcing to create major and rapid climate shifts at glacial-interglacial transitions.

Evidence on past Atlantic Ocean circulation derived from carbon isotope reconstructions has been used to suggest that ocean circulation is primarily responding to, rather than driving, Pleistocene climate change on orbital timescales. For example, *Imbrie et al*. [1992] placed deep Atlantic ventilation within a "late response" group of variables, with increased ventilation occurring ~8 kyr behind precessional maxima in Northern Hemisphere insolation. More recently, *Lisiecki et al*. [2008] similarly proposed a lag of 6–11 kyr

between that insolation forcing and Atlantic overturning, which they inferred from carbon isotope gradients between the mid-depth Atlantic and deep Pacific oceans. Such a significant lag between the insolation forcing and the circulation response would appear to place limits on the processes behind a Milankovitch mechanism for glacial cycles (i.e., control by summer insolation at 65°N), while some studies have suggested a significant role for Southern Hemisphere insolation instead [e.g., *Drysdale et al*., 2009]. However, carbon isotopes contain multiple signals from air-sea exchange, nutrient regeneration, and terrestrial carbon cycling, in addition to circulation, potentially making interpretation of those records ambiguous. The use of intra-oceanic carbon isotope gradients largely removes the effect of changing terrestrial carbon storage, but it is hard to resolve the combined effects of changes in water mass sourcing, end-member compositions, flow rates, and biological productivity through time.

In contrast, a mechanism has recently been proposed to explain glacial inception by calling upon an active role for the deep ocean, potentially driven by Northern Hemisphere insolation [*Adkins*, 2013]. This mechanism involves the interplay between the properties of NADW and Antarctic Bottom Water (AABW), because NADW upwells around Antarctica where it is transformed into the dense AABW which fills the deepest layers of the global ocean. The proposal is that a cooling of NADW would reduce the melting of Antarctic ice and lead to the formation of a saltier and denser version of AABW [*Miller et al*., 2012; *Adkins*, 2013]. This process would serve to increase the deep ocean density contrast and isolate the deep ocean from the mid-depths. The capacity of the deep ocean for carbon storage would be enhanced, which could lead on to further cooling and glaciation through a positive feedback. *Ferrari et al*. [2014] have also highlighted a link between Antarctic sea ice extent and the depth of the boundary between these northern-sourced ("NADW") and southern-sourced ("AABW") overturning cells that is controlled by the geometry of the Antarctic Circumpolar Current. With expanded glacial sea ice, the shoaled lower boundary of NADW would lie above the depths of rough seafloor topography, severely hindering vertical mixing between NADW and AABW and largely isolating these shallow and deep overturning cells [*Ferrari et al*., 2014; their Figure 4].

The above discussion highlights clear differences in existing views of the ocean-climate link. In part, this uncertainty may reflect the multiple controls on any single paleoceanographic proxy, leading to multiple possible interpretations of temporal changes. Multi-proxy studies should provide stronger constraints, and our approach takes advantage of the multiple and complementary controls on Nd and carbon isotopes as tracers of deep ocean circulation and chemistry. Since Nd isotopes are influenced by mixing between water masses but unaffected by air-sea exchange and biological cycling [*Frank*, 2002; *Goldstein and Hemming*, 2003], they are able to provide more robust evidence on the physical reorganization of ocean circulation. In addition, comparison between Nd and carbon isotope records may provide valuable insights into the relationship between ocean circulation and the carbon cycle [*Piotrowski et al*., 2005, 2009].

### 1.1. This Study

Circumpolar Deep Water (CDW) is formed by mixing between NADW, AABW, and Pacific waters in the Southern Ocean and ventilates large volumes of the global ocean, making it both an important carbon reservoir and a sensitive recorder of past circulation changes. In this study, we use Nd and carbon isotopes from deep Central Indian Ocean core SK129-CR2 to reconstruct the temporal evolution of CDW circulation and chemistry through the last two glacial cycles (0–250 ka B.P.), providing new constraints on the role of ocean circulation in glacial cycles.

Our contribution comprises two main elements. We first extend the existing SK129-CR2 sediment leachate Nd isotope record from the last glacial cycle [*Piotrowski et al*., 2009] through the penultimate glacial cycle and provide evidence to assess its reliability. We evaluate sediment leachate Nd isotope data by comparison to foraminifera and fish teeth data, and following recent evidence from the experimental study of *Wilson et al*. [2013] we propose a small correction to our new leachate data related to sample size. We further evaluate the corrected leachate data with measurements on non-decarbonated sediment leachates and by comparison to records from other cores. Overall, this aspect of our study provides (i) a demonstration of the need to understand the potential challenges when making Nd isotope reconstructions; (ii) validation of an approach proposed for more reliable sediment leaching [*Wilson et al*., 2013] applied here to a different setting; and (iii) robust support for a paleoceanographic interpretation of the extended record.

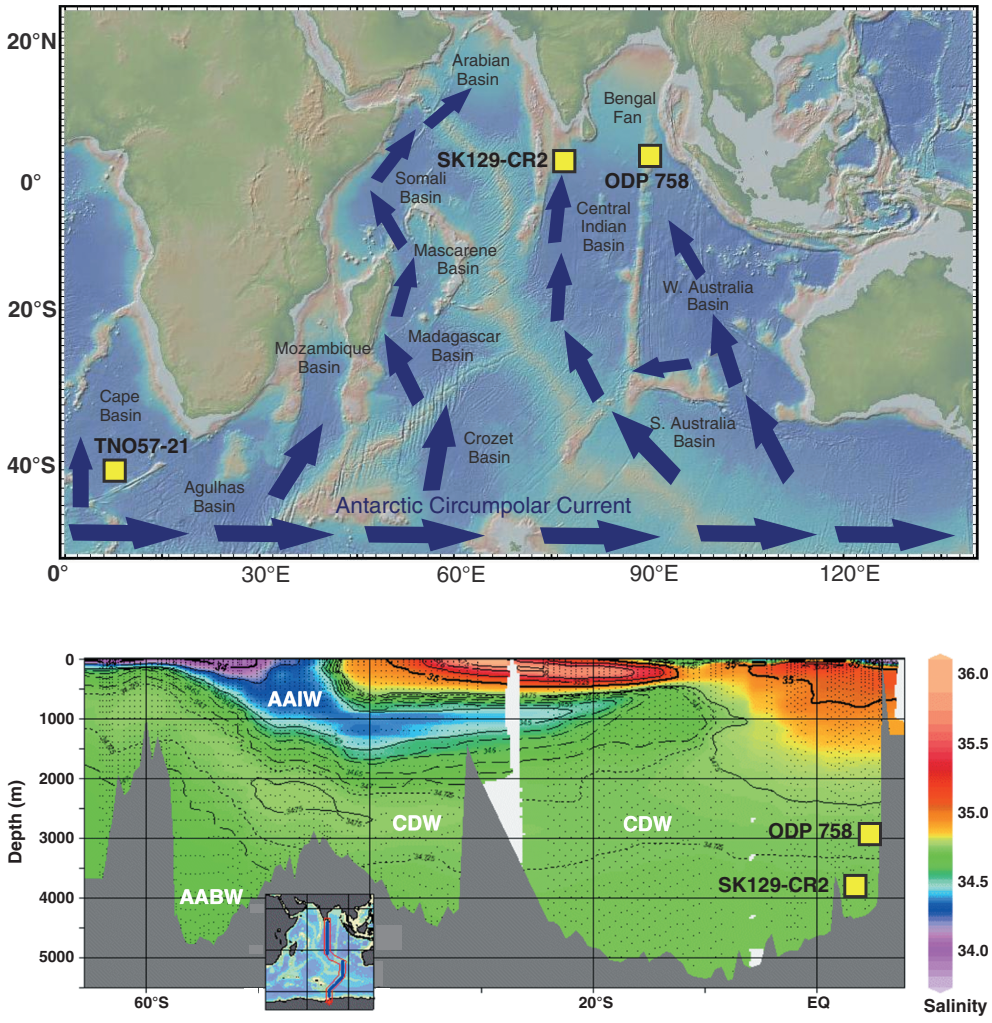


**Figure 1.** Location and hydrography of core SK129-CR2. (top) The generalized Indian Ocean deep water circulation, with northward advection shown in blue arrows. Yellow squares mark the locations of sediment cores SK129-CR2 (3800 m depth; this study), TNO57-21 (4981 m) [*Piotrowski et al.*, 2008, 2012], and ODP 758 (2934 m) [*Gourlan et al.*, 2010]. Base map from GeoMapApp. (bottom) A south-north hydrographic section, with salinity data from eWOCE and major water masses labeled (CDW = Circumpolar Deep Water, AABW = Antarctic Bottom Water, and AAIW = Antarctic Intermediate Water).

In the subsequent part, we use this Nd isotope record, together with new and existing benthic carbon isotope data from the same core, to assess the timing and role of ocean circulation changes in glacial cycles. Our record spans two full glacial cycles, allowing us to assess potential orbital controls, and in particular the stronger precessional insolation forcing related to eccentricity modulation during the penultimate glacial cycle. By interrogating this record, we provide new evidence on the link between orbital forcing and ocean circulation, and insight into the role of ocean circulation in glacial inceptions, within glacial periods and across glacial-interglacial cycles.

## 2. Regional Setting and Hydrography

We reconstruct the evolving chemistry of CDW through time using Indian Ocean sediment core SK129-CR2 (3°N, 76°E, 3.8 km water depth; hereafter SK129) [*Banakar*, 2005]. This core is located on the eastern side of the Chagos-Laccadive ridge in the Central Indian Basin (Figure 1) and is ventilated by Upper CDW from the Southern Ocean [*Mantyla and Reid*, 1995; *You*, 2000]. Maps of potential density surfaces show that this water is derived from Southern Ocean depths of ~1.5–3 km [*Mantyla and Reid*, 1995] and sinks to deeper depths northward into the Indian Ocean (Figure 1). The total deep water inflow to the Indian Ocean is estimated to be 11 ± 4 Sverdrups [*Ganachaud et al.*, 2000], distributed between western and central

branches, the latter of which supplies deep waters to the location of SK129 [*You*, 2000]. Circumpolar Deep Water from the South Australia Basin can reach the Central Indian Basin by a direct route via a gap between the Southeast Indian Ridge and the Broken Plateau (~34°S, 83°E) and by an indirect route via the West Australia Basin and gaps in the Ninety East Ridge at ~33°S and ~28°S [*Mantyla and Reid*, 1995] (Figure 1). A deep western boundary current in the Central Indian Basin [*You*, 2000] is responsible for the subsequent northward transport towards core SK129 in the northern Indian Ocean.

## 3. Materials and Methods

### 3.1. Sampling

Neodymium isotopes were measured on bulk decarbonated sediment leachates from 40 samples in SK129 (320–512 cm core depth; ~158–249 ka B.P.) in order to extend the MIS 1–5 Nd isotope record of *Piotrowski et al*. [2009] to the end of MIS 8. Neodymium isotopes were also measured on fish teeth and bones from six samples within MIS 6–7, and on uncleaned planktonic foraminifera from nine samples across MIS 1–8. A further 12 sediment leachate samples were analyzed from MIS 6–8 following a modified procedure using smaller solution/solid ratios to prevent complete decarbonation of the sediments before the reductive leaching [*Wilson et al*., 2013]. Benthic foraminiferal carbon ($\delta^{13}C$) and oxygen ($\delta^{18}O$) isotopes were measured on *Cibicidoides wuellerstorfi* in 64 samples, mostly from MIS 6–8, to extend the existing MIS 1–5 record [*Piotrowski et al*., 2009].

### 3.2. Sediment Leaching

Acid-reductive leaching of bulk sediment aims to extract Nd from the authigenic ferromanganese oxyhydroxide coatings on detrital and biogenic grains [*Chester and Hughes*, 1967; *Bayon et al*., 2002; *Gutjahr et al*., 2007; *Martin et al*., 2010]. Briefly, bulk sediment samples of ~5–10 $cm^3$ volume were leached in 30 mL 0.44 M acetic acid solution (buffered to pH 5 by sodium acetate) in 50 mL centrifuge tubes on a rotating wheel at room temperature. This process was repeated 9–11 times over 14–24 days until carbonate had been removed from all samples. Samples were washed at least twice with deionized water, before the ferromanganese oxides were recovered by acid-reductive leaching for 1 h in 30 mL of a pH 2 solution of 0.02 M hydroxylamine hydrochloride (HH) in 4.4 M acetic acid. This HH leachate was centrifuged at 5000 rpm and decanted 3 times in sequence to prevent the transfer of detrital particles, before chemical separation and mass spectrometry. For 12 samples, we carried out a modified leaching procedure [after *Wilson et al*., 2013], with a shorter period of buffered acetic acid leaching (3–4 times over 6 days) so that these samples were not fully decarbonated before the HH leaching.

### 3.3. Uncleaned Foraminifera

Uncleaned foraminifera (i.e., cleaned of detritus but not chemically cleaned) may also be used as a substrate for reconstructing bottom water Nd isotope compositions [*Palmer and Elderfield*, 1985; *Roberts et al*., 2010; *Piotrowski et al*., 2012], and our methodology followed *Roberts et al*. [2010]. Briefly, bulk sediment samples were wet sieved (>63 μm), and mixed species of planktonic foraminifera were picked from the > 355 μm fraction to give sample sizes of 30–100 mg. The foraminifera were crushed between glass plates, and fine clays and detrital silicates were removed by repeated sonication and pipetting until the water remained clear. The samples were examined under a microscope and, where necessary, any remaining detrital grains were removed with a fine brush, although the detrital content of the samples was negligible in all cases. After washing with deionized water, 0.5 mL of deionized water was added followed by up to 1 mL of 1 M acetic acid over a period of a few hours until the crushed foraminifera fragments had dissolved.

### 3.4. Fish Teeth

Fish teeth and fish debris record bottom water Nd isotopes because they acquire their Nd from bottom water (or shallow pore water) shortly after deposition [*Staudigel et al*., 1985; *Martin and Haley*, 2000]. For this study, fish teeth (and occasionally fish debris) were picked from the > 212 μm fraction to give sample sizes of 10–200 μg. The fish teeth were cleaned according to the reductive cleaning step (hydrazine, ammonia, and citric acid mixture) of *Boyle and Keigwin* [1985], but with the oxidative step omitted, as in *Roberts et al*. [2010]. In support of this approach, *Martin et al*. [2010] recently suggested that an extensive cleaning procedure involving both oxidative and reductive steps is unnecessary in typical pelagic sediments.

### 3.5. Elemental Separation and Mass Spectrometry for Nd Isotopes

For all samples, the rare earth element fraction was separated using Eichrom TRUspec™ resin (100–150 μm mesh) in 100 μl Teflon columns, and the Nd fraction was isolated using Eichrom LNspec™ resin (50–100 μm mesh) on volumetrically calibrated Teflon columns. The Nd isotopic composition was analyzed on the Nu Plasma multi-collector inductively-coupled plasma mass spectrometer in the Department of Earth Sciences at the University of Cambridge, using an exponential mass fractionation correction (to $^{146}Nd/^{144}Nd = 0.7219$) and standard–sample bracketing with concentration-matched JNdi-1 standard [*Tanaka et al*., 2000]. Data are expressed in $\varepsilon_{Nd}$ notation as the deviation in parts per 10,000 from the present-day composition of the Chondritic Uniform Reservoir ($^{143}Nd/^{144}Nd = 0.512638$) [*Jacobsen and Wasserburg*, 1980; *Wasserburg et al*., 1981]. Data were collected in a number of analytical sessions, and measurement uncertainty is given by the within-session standard deviation (2σ) on concentration-matched JNdi-1 standards. For samples analyzed in duplicate, the reported values are the mean, weighted according to the variance, and the 2σ standard error. Typical external reproducibility for 25 ng of Nd is ~0.3 $\varepsilon_{Nd}$ units, while larger errors for some foraminifera or fish teeth samples reflect low Nd abundance due to small sample sizes.

### 3.6. Foraminiferal Stable Isotopes

Benthic foraminiferal $\delta^{18}O$ and $\delta^{13}C$ were measured in the Godwin Laboratory on *Cibicidoides wuellerstorfi* (>212 μm). Foraminifera (typically 2 to 5 specimens) were transferred into sample vials, crushed, and soaked in a solution of 3% hydrogen peroxide for 30 min before being removed. After an acetone ultrasonic bath, the samples were dried at 50°C overnight. The samples were analyzed using a Micromass Multicarb Sample Preparation System attached to a VG SIRA or VG PRISM mass spectrometer. Each run of 30 samples was accompanied by 10 reference carbonates and two control samples. The results are reported with reference to the international standard Vienna Pee Dee Belemnite, and the precision is better than ± 0.06‰ for $\delta^{13}C$ and ± 0.08‰ for $\delta^{18}O$.

### 3.7. Age Model

An age model for MIS 1–5 in SK129 was presented by *Piotrowski et al*. [2009], based on radiocarbon dates for 0–34 ka, beyond which the benthic foraminiferal (*C. wuellerstorfi*) $\delta^{18}O$ shifts at the MIS 6–5 and MIS 5–4 boundaries were tuned to SPECMAP $\delta^{18}O$ [*Martinson et al*., 1987]. That age model has been updated and extended (Tables S1–S3) using correlation of benthic $\delta^{18}O$ to the LR04 benthic $\delta^{18}O$ stack [*Lisiecki and Raymo*, 2005] at major MIS boundaries and linear interpolation between tie points. The first appearance of abundant Youngest Toba Tuff shards at ~75 ka (160 cm) [*Banakar*, 2005] provides an independent chronological tie point that is in good agreement with the LR04-based tie points.

The LR04 stack is based on orbital tuning to Northern Hemisphere insolation calculations, with a phase lag of ~3 kyr for precession and ~7 kyr for obliquity over the 0–250 ka section of the stack, and has an estimated maximum absolute age error of ~4 kyr over this period [*Lisiecki and Raymo*, 2005]. Since good agreement is achieved between the SK129 $\delta^{18}O$ record and the LR04 $\delta^{18}O$ stack with relatively few tie points (Table S2), we suggest that a similar chronological error applies to our SK129 record (while such age model uncertainty does not affect the relative phasing of signals recorded by different proxies in SK129 itself). Lags of ~2 kyr have been observed in benthic $\delta^{18}O$ records between Atlantic and Pacific Ocean records at terminations and attributed to a combination of ocean transit times and diachronous hydrographic changes [*Skinner and Shackleton*, 2005; *Lisiecki and Raymo*, 2009], but such processes would have a minor effect at the resolution of our record. Therefore, we should be able to investigate both glacial-interglacial and orbital timescale proxy variability in SK129, but we cannot expect to resolve the exact phasing with respect to insolation forcing.

## 4. Reliability of Nd Isotope Reconstructions

The sediment leachate Nd isotope data presented here are a compilation of new and existing data (Table S4). The leachate data from MIS 1–5 are decarbonated sediment leachates from *Piotrowski et al*. [2009]. For MIS 6–8, decarbonated sediment leachate data were collected in this study following a similar procedure. However, we have demonstrated in parallel studies that artifacts can arise during sediment leaching for Nd isotopes [*Piotrowski et al*., 2012; *Wilson et al*., 2013], in particular related to the decarbonation step that precedes reductive leaching. We suggested that comparison with Nd isotope data from contemporaneous

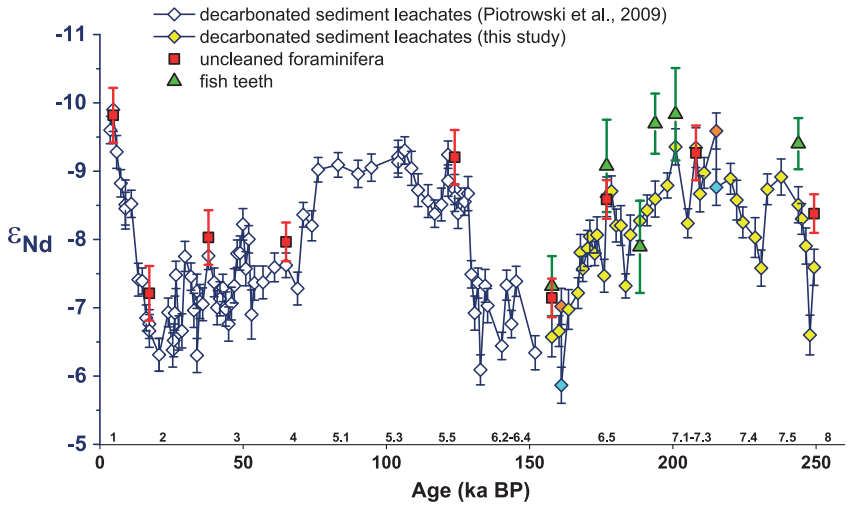


**Figure 2.** Comparison of Nd isotope data by different methods plotted versus age: decarbonated sediment leachates [*Piotrowski et al.*, 2009], decarbonated sediment leachates (this study), uncleaned foraminifera and fish teeth. The orange and blue diamonds in the decarbonated sediment leachate record at ~161 ka and ~215 ka represent large and small sample sizes, respectively (see Table S4). Numbers along the *x* axis are MIS numbers.

foraminifera or fish teeth may be the best way to assess sediment leachate data, and that leaching sediments before they have been completely decarbonated (i.e., non-decarbonated sediment leachates) may provide a more reliable approach [*Wilson et al.*, 2013]. We also showed that those artifacts were highly systematic, raising the possibility of correcting existing decarbonated leachate data for this artifact.

Below we evaluate the reliability of the decarbonated leachate data in SK129 from both the previous study [*Piotrowski et al.*, 2009] and the present study, using supporting evidence from fish teeth, uncleaned foraminifera, and non-decarbonated sediment leachates. We demonstrate that (i) our decarbonated leachate data from SK129 are slightly but not significantly affected by leaching artifacts such as those we have previously described; (ii) those leachate data are improved by a correction based on the sample size leached; (iii) the corrected decarbonated leachate data can be validated and extended with additional non-decarbonated leachate measurements; and (iv) the final composite record is in excellent agreement with an existing low-resolution record from the Central Indian Ocean [*Gourlan et al.*, 2010], as well as the Cape Basin record for the period of overlap [*Piotrowski et al.*, 2008, 2012].

### 4.1. Comparison Between Decarbonated Leachates, Foraminifera, and Fish Teeth

Measurements of Nd isotopes on uncleaned foraminifera from MIS 1–8 (Table S5) are generally in agreement with decarbonated sediment leachate data, with seven out of nine samples agreeing within error (Figure 2). Within MIS 6–7, data from fish teeth (Table S5) are within error of the decarbonated sediment leachate data in three out of six cases (Figure 2). It may be possible to explain occasional discrepancies by differences in the depth within the sediment at which the Nd isotope signal is recorded by the different phases, or by a grain-size dependent response to bioturbational mixing [*Heinze et al.*, 2009], but such processes might be expected to produce random variability. Instead, the decarbonated leachates are systematically more radiogenic than those other two substrates, with a mean offset of 0.3 $\varepsilon_{Nd}$ units (maximum of 0.8 $\varepsilon_{Nd}$ units) compared to the contemporaneous foraminifera (MIS 1–8) and a mean offset of 0.6 $\varepsilon_{Nd}$ units (maximum of 1.1 $\varepsilon_{Nd}$ units) compared to contemporaneous fish teeth (MIS 6–7). This systematic difference is significantly smaller than the glacial-interglacial variability of ~3 $\varepsilon_{Nd}$ units (Figure 2) but is significant compared to analytical uncertainty of ~0.3 $\varepsilon_{Nd}$ units. Therefore, we suggest that the decarbonated leachates in SK129 are influenced by a small degree of contamination by a minor volcanic component with a radiogenic Nd isotopic composition, similar to previous observations from a suite of cores in the western Indian Ocean [*Wilson et al.*, 2013].

### 4.2. Sample Size Correction for Decarbonated Leachates

We previously showed that the use of small sample sizes in the conventional decarbonated leaching procedure can lead to a shift away from seawater compositions towards more radiogenic Nd isotopic

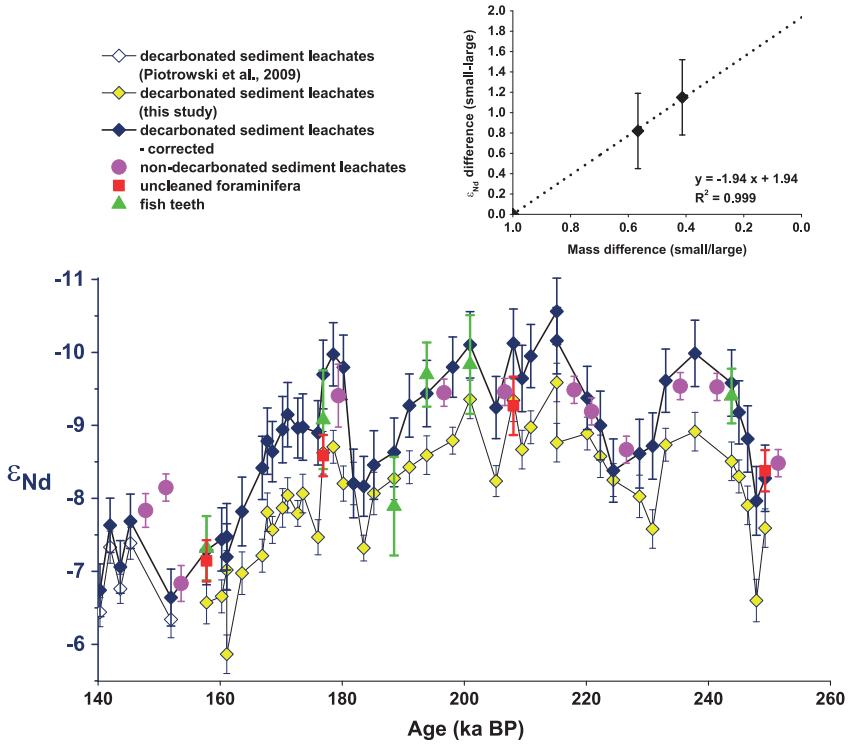


**Figure 3.** Neodymium isotope data from decarbonated sediment leachates in MIS 6–8 (*Piotrowski et al.* [2009] and this study) before and after correction as described in the main text. These data are compared to Nd isotopes from non-decarbonated sediment leachates, uncleaned foraminifera, and fish teeth (this study). The inset graph shows the basis for the leachate sample size correction based on sample size tests at ~161 ka and ~215 ka (see Table S4 and Figure 2), with error bars representing propagated 2σ.

compositions [*Wilson et al.*, 2013]. We make the same observation here from sample size tests at two core depths in SK129 (161 ka and 215 ka; Figure 2), with an increase in Nd isotopic composition in proportion to the mass difference (ratio) between samples (Figure 3 inset). We further suggest that these data provide a useful basis to correct the decarbonated leachate data collected in this study (Figure 3). Since all samples underwent a similar number of buffered acetic acid leaching steps, we focus only on sample size for our correction and all leachate data are size-corrected to the size of the largest sample (~6 g at ~182 ka). Although that choice is empirical, the rationale is that samples underwent repeated buffered acetic acid leaching in batches until all samples had been decarbonated, such that the largest samples (typically ~5–6 g in size) typically took the longest time to reach this point and should be closest to recording the most robust authigenic signature. For smaller samples, the buffered acetic acid leaching employed was excessive to decarbonate the sediment, leading to a shift towards more radiogenic Nd isotopic compositions. We assume that the uncertainties for the points on the calibration plot (i.e., 0.37 $\varepsilon_{Nd}$ units; Figure 3 inset) dominate the uncertainty on this correction and propagate this uncertainty together with the analytical uncertainty on each individual sample measurement to give our final uncertainty.

Unfortunately, sample sizes are not available from the *Piotrowski et al.* [2009] study; and in that case, we use a simple empirical correction to the leachate data (an offset of $0.3 \pm 0.3$ $\varepsilon_{Nd}$ units) that leads to the best agreement between the leachate and foraminiferal Nd isotopes at the five depths in MIS 1–5 where both were measured (Figure 2). Fortunately, this correction is small (on the scale of the external analytical reproducibility) and therefore does not impact in any significant way on the previous interpretation of that record.

Those two correction procedures lead to a significant improvement in the consistency between decarbonated sediment leachate data and foraminiferal and fish teeth data (Figure 3). In 9 out of 13 cases, the correction improves the agreement between leachate data and contemporaneous foraminifera or

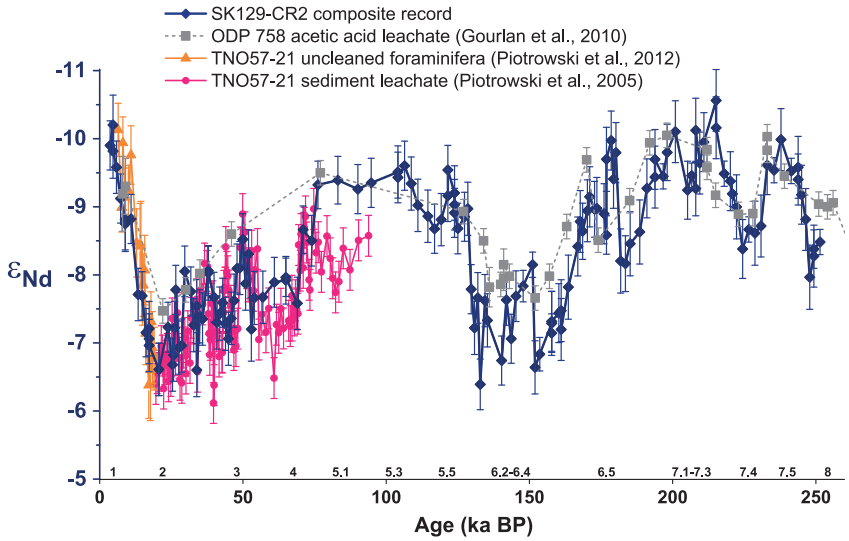


**Figure 4.** Composite SK129 Nd isotope record (including non-decarbonated leachates, corrected decarbonated leachates, foraminifera, and fish teeth) in comparison to records from Indian Ocean site ODP 758 (acetic acid leachates; *Gourlan et al.* [2010]; see Figure 1 for location) and Cape Basin TNO57-21 (foraminiferal coatings [*Piotrowski et al.*, 2012] and sediment leachates [*Piotrowski et al.*, 2005]; see Figure 1 for location). The ODP 758 record has a lower resolution than SK129-CR2 and is plotted on its own published age scale, so perfect agreement between the two records through time would not be expected. All data from SK129 are included, with the exception of fish teeth data from three depths which are in agreement with the other data but have significantly larger analytical uncertainties (0.68 $\varepsilon_{Nd}$ units) reflecting small sample sizes. Numbers along the *x* axis are MIS numbers.

fish teeth data, and after the correction, 12 out of 13 corrected leachate values are within error of contemporaneous foraminifera or fish teeth data.

### 4.3. Evidence From Non-decarbonated Leachates

In order to provide an additional test for the reliability of that corrected leachate record, we also measured non-decarbonated sediment leachates on 12 further samples within MIS 6–7, following the recommendations of *Wilson et al.* [2013], i.e., lower solution/solid ratios and shorter buffered acetic acid leaching times in order to prevent complete decarbonation prior to the HH leaching. That procedure relies upon the fact that biogenic carbonate acts as a low-Nd carrier phase for the authigenic Nd isotopes acquired from bottom water [*Roberts et al.*, 2012; *Tachikawa et al.*, 2014] and was demonstrated to minimize the potential for leaching artifacts [*Wilson et al.*, 2013]. Unlike the uncorrected decarbonated sediment leachate data, those non-decarbonated sediment leachate data are in excellent agreement with data from both fish teeth and foraminifera (Figure 3), supporting their reliable seawater origin. Furthermore, there is an excellent agreement (within ~0.2 $\varepsilon_{Nd}$ units) between the measured data from the non-decarbonated leachates and the corrected data from the decarbonated leachates (Figure 3). These observations are quite striking and strongly support the robustness of our sample size correction for the decarbonated leachates, despite the fact that our calibration was based on only two points (Figure 3 inset). It is also clear that the uncorrected decarbonated leachate data differ significantly from the non-decarbonated leachate data (Figure 3), providing a clear indication of the need for our sample size correction.

Given the above evidence, we consider that both leaching approaches (i.e., size-corrected decarbonated leachates and non-decarbonated leachates) provide a reliable and consistent reconstruction of past bottom water Nd isotopic compositions in SK129. By combining the data from the two approaches, in addition to the data from foraminifera and fish teeth, we increase the resolution of the record to approximately one sample every 2 kyr through MIS 6–7 (Table S6). However, we emphasize that future studies should continue to explore a simple one-step extraction technique, without the prior removal of carbonates, to remove the need for such an empirical correction.

### 4.4. Comparison of SK129 Nd Isotope Record to Records From Other Cores

In Figure 4, we present the composite SK129 Nd isotope record, incorporating data from sediment leachates, foraminifera, and fish teeth. The reliability of that composite record is independently assessed by comparison

to a low-resolution Nd isotope record from nearby site Ocean Drilling Program (ODP) 758 [*Gourlan et al*., 2010] (see Figure 1 for location). That study used a single-step acetic acid leaching procedure to extract the authigenic phases and is therefore considered to be robust [*Wilson et al*., 2013]. There is an excellent agreement of both absolute values and temporal variability between the two records (Figure 4), as expected for two cores that both sample CDW at present (albeit at slightly different water depths), and that agreement also suggests that these cores sampled similar water masses throughout past glacial-interglacial cycles.

The original Cape Basin (TNO57-21) record was based on decarbonated sediment leachates [*Piotrowski et al*., 2008] but is considered reliable since its major features are well supported by uncleaned foraminifera data across the last deglaciation [*Piotrowski et al*., 2012]. The similarity between the Cape Basin (TNO57-21) and SK129 Nd isotope records for the period of overlap (Figure 4) further supports the reliability of the new Indian Ocean record and is consistent with all cores providing evidence on the Nd isotopic variability of CDW in the Southern Ocean.

Overall, the above evidence from multiple authigenic phases and the inter-core comparison demonstrates the care that is required in evaluating Nd isotope records obtained by chemical extraction techniques and provides support for the reliability of the record presented here.

## 5. Circumpolar Deep Water Chemistry Through Two Glacial Cycles

In this section, we briefly summarize our new evidence from SK129 on the temporal evolution of CDW chemistry through the last two glacial cycles, before discussing detailed explanations and potential climate implications in section 6.

### 5.1. Carbon Isotopes

Benthic carbon isotopes in SK129 show glacial-interglacial variations of ~0.7‰ (Figure 5c), approximately twice as large as the deglacial whole-ocean change related to carbon budget reorganization [*Tagliabue et al*., 2009], indicating additional controls such as from water mass sourcing or nutrient cycling. Both the temporal pattern and absolute values recorded in SK129 are similar to western Indian Ocean and southwest Pacific Ocean $\delta^{13}C$ records (Figure 5c), consistent with continuous ventilation by CDW at these sites. We also observe a long-term trend in $\delta^{13}C$, such that consecutive glacials and consecutive interglacials do not have the same values but instead increase by 0.3–0.4‰ from 250 ka towards the present (Figure 5c). This trend occurs over longer timescales than glacial-interglacial cycles and is consistent with previous observations of whole-ocean $\delta^{13}C$ changes that have been attributed to changes in the terrestrial carbon budget and/or global carbon cycle [e.g., *Wang et al*., 2004; *Martinez-Mendez et al*., 2008].

### 5.2. Neodymium Isotopes

Neodymium isotopes from authigenic phases in SK129 provide evidence on past bottom water composition, revealing Nd isotopic variations that are consistent between successive interglacials ($\varepsilon_{Nd} \sim -9.5$ to $-10$) and glacials ($\varepsilon_{Nd} \sim -6.5$ to $-7$) (Figure 5b). The warmer substages of MIS 3 ($\varepsilon_{Nd} \sim -8.5$) and MIS 6.5 ($\varepsilon_{Nd} \sim -9.5$) also approach those interglacial values. Both the magnitude of change and absolute values at SK129 are strikingly similar to the Cape Basin record for the period of overlap [*Piotrowski et al*., 2008, 2012] (Figure 5b), suggesting similar water mass sourcing at those sites through time. Since the modern day composition of Southern Ocean waters can be explained by mixing between NADW ($\varepsilon_{Nd} \sim -13$) and Pacific ($\varepsilon_{Nd} \sim -4$) sources [*Stichel et al*., 2012], the more radiogenic Nd isotopic compositions recorded during glacial periods suggest a reduced presence of NADW in the glacial Southern Ocean.

### 5.3. Sawtooth and Square Wave Expressions of the Glacial Cycle

On glacial-interglacial timescales, the simplest interpretation of the combined Nd isotope and $\delta^{13}C$ changes in SK129 involves a reduced NADW component in the glacial Southern Ocean and a higher nutrient content (Figure 5), but it is clear that the glacial cycle is expressed differently by these two tracers. To a first order, for each of the last two glacial cycles, the $\delta^{13}C$ record resembles a square wave, with the lowest values recorded during both early and late glacial periods (Figure 5c). In contrast, Nd isotopes continue to evolve from $-8$ to $-6.5$ between early and late glacial periods, producing a sawtooth pattern for each of the last two glacial cycles (Figure 5b).

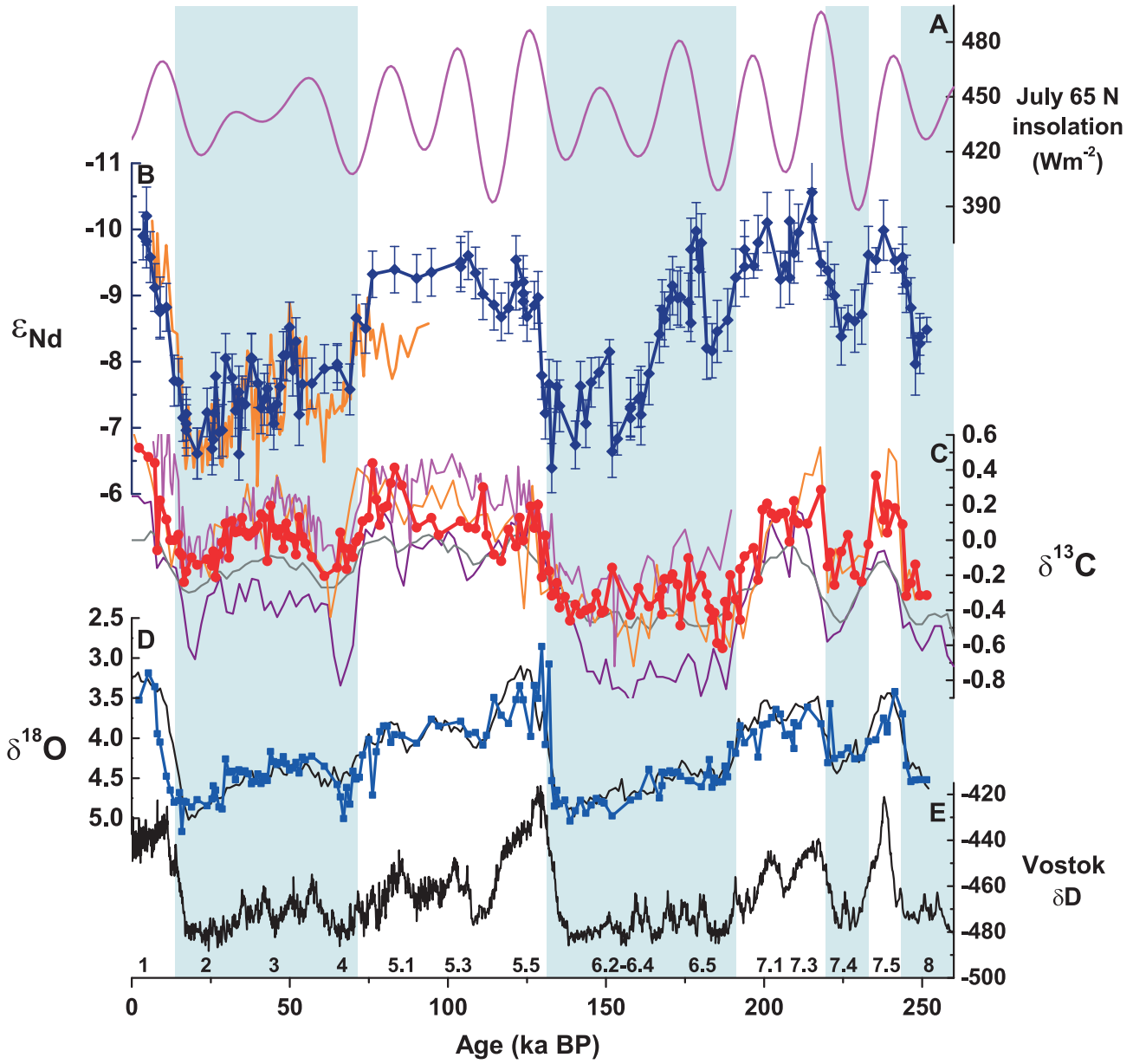


**Figure 5.** Indian Ocean Nd isotope, $\delta^{13}C$, and $\delta^{18}O$ records in a global context. (a) Northern Hemisphere summer insolation at 65°N [*Berger and Loutre*, 1991]. (b) SK129 Nd isotope record (blue diamonds and line), plotted on a reversed axis with 2σ uncertainties and compared to Nd isotope data from the Cape Basin core TNO57-21 (orange line) [*Piotrowski et al.*, 2008, 2012]. (c) SK129 benthic $\delta^{13}C$ (red circles and line) compared to western Indian Ocean core WIND 28K (pink line) [*McCave et al.*, 2005], southwest Pacific core ODP 1123 (orange line) [*Hall et al.*, 2001], Pacific Deep Water stack (grey line) [*Lisiecki*, 2010], and Southern Component Water stack (purple line) [*Lisiecki*, 2010]. All records are from *C. wuellerstorfi*, except for that from ODP 1123 which was measured on *Uvigerina* species and is plotted as *Cibicidoides* equivalent (+0.8). (d) SK129 benthic $\delta^{18}O$ (blue squares and line) plotted on a reversed axis after adjusting to equilibrium values (+0.64), together with the LR04 $\delta^{18}O$ stack (black line) [*Lisiecki and Raymo*, 2005]. (e) Vostok δD [*Petit et al.*, 1999] on the GT4 age scale (black solid line). Blue shaded bars highlight glacial periods. Numbers along the *x* axis are MIS numbers.

### 5.4. Precessional Variability in Nd Isotopes

In addition to glacial-interglacial Nd isotope variability, we also observe a precession signal in our Nd isotope record that is approximately in phase with Northern Hemisphere summer insolation (Figure 6a). Time series analysis reveals that the precession signature is statistically significant when considering the record in its entirety (Figure 7c). In detail, wavelet analysis shows that the precession signal in Nd isotopes is strongest in MIS 6–7 (Figure 7b), whereas there is not a significant precession signal during MIS 2–4. These differences between the last two glacial cycles appear to correspond to differences in the insolation

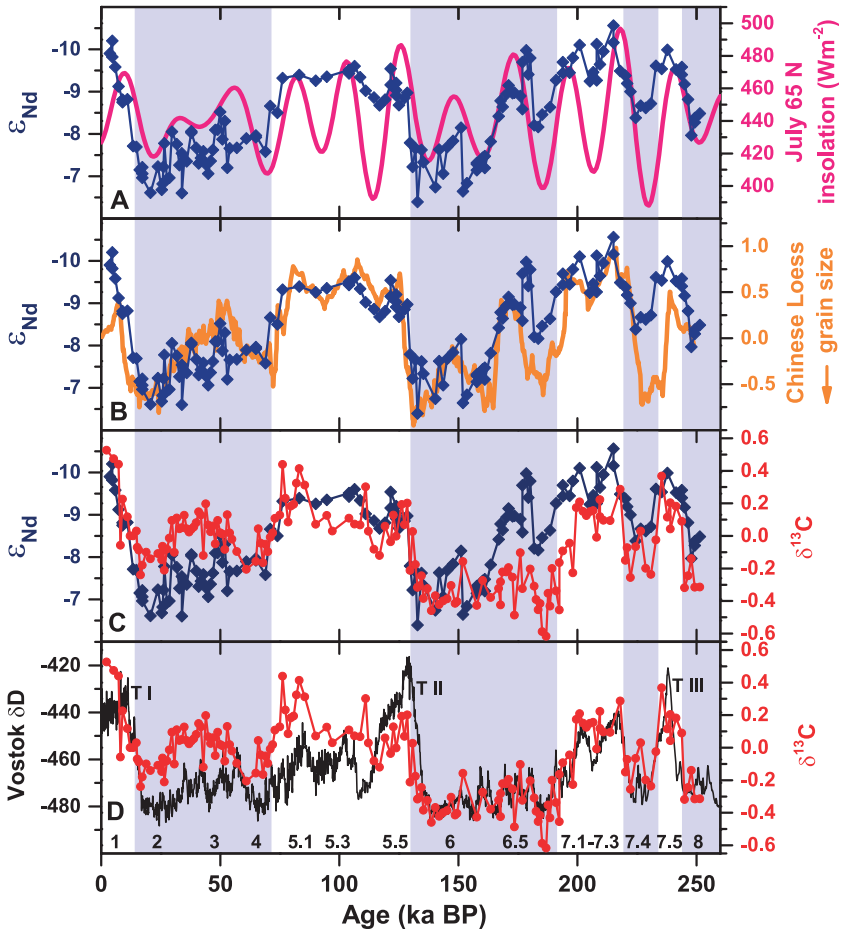


**Figure 6.** SK129 Nd isotope and benthic $\delta^{13}C$ records compared to each other and to other palaeoclimate records. (a) Northern Hemisphere summer insolation (W $m^{-2}$) at 65°N [*Berger and Loutre*, 1991] and $\varepsilon_{Nd}$. (b) Chinese Loess grain size (normalized stack; positive = finer grain size) [*Yang and Ding*, 2014] and $\varepsilon_{Nd}$. (c) Benthic $\delta^{13}C$ and $\varepsilon_{Nd}$. (d) Benthic $\delta^{13}C$ and Vostok δD [*Petit et al.*, 1999]. Blue shaded bars highlight glacial periods. Numbers along the *x* axis are MIS numbers. Labels T I, T II, and T III indicate glacial terminations.

forcing, since the precession component in the insolation forcing is also strongest in MIS 6–7 and rather subdued during MIS 2–4 (Figure 6a). A precession signal in Nd isotopes is also not observed during the latter part of MIS 5, which may imply a reduced sensitivity to precession forcing within interglacial periods, but the Nd isotope record is at its lowest resolution during late MIS 5, and this observation may need to be addressed by more data in the future.

## 6. Discussion

### 6.1. Neodymium Isotopes as a Water Mass Tracer in the Indian Ocean

In Figure 8, we plot seawater Nd isotopes versus salinity for the modern mid-depth and deep oceans, focusing on the Southern Ocean and Indian Ocean. Seawater in the southeast Atlantic Ocean and Southern Ocean falls within a mixing window defined by CDW in the Drake Passage ($\varepsilon_{Nd} \sim -8.5$) [*Stichel et al.*, 2012] and NADW in the North Atlantic ($\varepsilon_{Nd} \sim -13$) [*Piepgras and Wasserburg*, 1987]. With the exception of the densest forms of AABW, whose composition is influenced to some extent by Nd inputs from the Antarctic shelves [*Stichel et al.*, 2012; *Rickli et al.*, 2014], a number of studies have indicated an otherwise negligible role for local Nd inputs in the Southern Ocean [*Carter et al.*, 2012; *Stichel et al.*, 2012]. Our late Holocene data from SK129 also fit within that mixing window (Figure 8), in particular corresponding closely to those NADW/CDW mixtures recorded in the southeast Atlantic sector of the Southern Ocean [*Stichel et al.*, 2012] and the deep Cape Basin [*Rickli et al.*, 2009]. This observation indicates the relatively conservative behavior of Nd isotopes in mid-depths of the

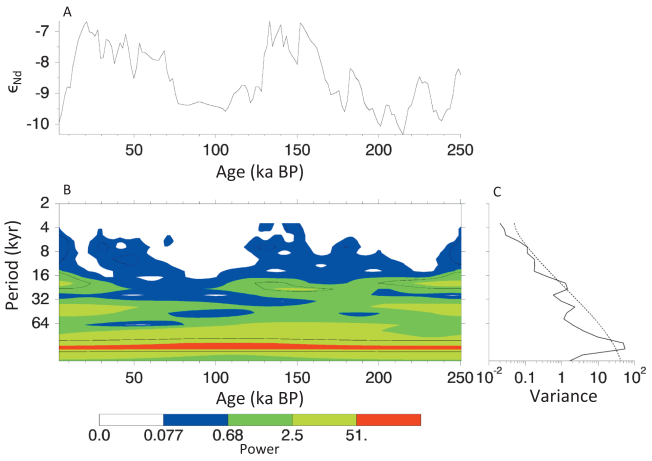


**Figure 7.** Time series analysis of the SK129 $\varepsilon_{Nd}$ record. The data were interpolated at 1.7 kyr resolution between 4 ka and 250.5 ka and then subject to wavelet analysis using the software on http://paos.colorado.edu/research/wavelets, based on *Torrence and Compo* [1998]. (a) SK129 $\varepsilon_{Nd}$ record (scale reversed compared to Figures 2–6). (b) Wavelet power spectrum: the contour levels are chosen so that 75%, 50%, 25%, and 5% of the wavelet power are above each level, respectively; black contour is the 5% significance level, using a red noise (autoregressive lag 1) background spectrum. (c) Global wavelet power spectrum (black line) compared to 5% significance level for red noise (dashed line). Note the significant peaks present at ~100 kyr and ~23 kyr periods.

Southern Ocean and Central Indian Ocean and the viability of Nd isotopes as a water mass tracer for this region. Conservative propagation of water mass signatures within and between the Southern Ocean and Indian Ocean was also previously suggested from ferromanganese crust and nodule data [*Albarede et al.*, 1997] and modeling studies [*Rempfer et al.*, 2012; *Friedrich et al.*, 2014].

There are two caveats to that simple picture, but they do not appear to appreciably influence our above conclusion. First, although Nd isotopes in the Southern Ocean and Indian Ocean appear to be well explained by mixing (Figure 8), Nd concentrations in both the deep Cape Basin [*Rickli et al.*, 2009] and the deep Indian Ocean [*Singh et al.*, 2012] are greater than in those NADW and CDW end-members. This observation likely reflects the non-conservative behavior of this tracer caused by particle scavenging, sometimes described as the "Nd paradox" [*Goldstein and Hemming*, 2003]. However, particle scavenging only appears to dominate the Nd isotope distribution in the Pacific Ocean [*Siddall et al.*, 2008; *Rempfer et al.*, 2011], which has been attributed to the influence of sluggish advection and abundant volcanic inputs, and should not impact significantly on the ability of Nd isotopes to trace water mass mixing in the region of our study.

Second, we consider the implications of recent studies that demonstrate an influence of local inputs on Nd isotopes in the northern Indian Ocean [*Singh et al.*, 2012; *Goswami et al.*, 2014]. Deep waters in the northern Bay of Bengal are clearly imprinted by highly unradiogenic Nd inputs from a Himalayan source [*Colin et al.*, 1999; *Singh et al.*, 2012] (Figure 8), likely through boundary exchange on the Bengal Fan, but that influence appears to be restricted to upper- and mid-fan settings. For example, deep water data from the most southerly Bay of Bengal site of *Singh et al.* [2012] at 6°N also fits within the $\varepsilon_{Nd}$-salinity mixing envelope (Figure 8), restricting the potential imprint from unradiogenic Himalayan inputs to be no more than ~0.5 $\varepsilon_{Nd}$ units at that location. Since SK129 is more distal than that site, any influence of local Nd sources here is likely even smaller, making it comparable to our analytical uncertainty. Therefore, the potential of such local sources to generate significant temporal changes in Nd isotopes at SK129 appears to be minor, especially since the modern Himalayan inputs are likely close to their maximum across glacial-interglacial cycles [*Lupker et al.*, 2013].

Figure 8 also allows us to emphasize a second important point for interpreting our Nd isotope record from SK129, which is that the deep Indian Ocean has a higher salinity than deep waters in the Drake Passage, with incomplete mixing in the Southern Ocean allowing a greater proportion of deep waters of Atlantic origin to reach this basin. It is clear from the seawater study of *Stichel et al.* [2012, their Figure 6] that the unradiogenic Nd isotope signature of NADW in the southeast Atlantic sector of the Southern Ocean ($\varepsilon_{Nd}$ values of −10 to −11 in the tongue of NADW at 2–3 km depth between 42°S and 47°S) may be propagated eastward within the northern part of the Antarctic Circumpolar Current. Although there are no published seawater Nd isotope measurements from the Indian sector of the Southern Ocean, two measurements from the deep western boundary current of the southwest Pacific Ocean ($\varepsilon_{Nd}$ values of −9.0 to −10.3 at 3.1–3.4 km depth, Figure 8) [*Molina-Kescher et al.*, 2014] have been linked to a remnant of NADW within the Antarctic Circumpolar Current. In that context, similar Nd isotope compositions for the

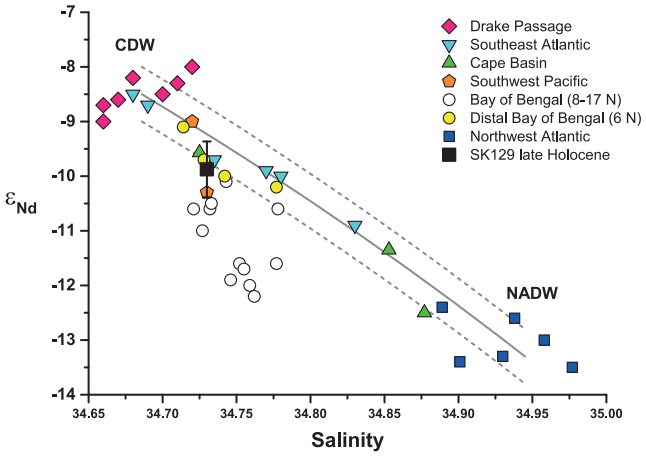


**Figure 8.** Seawater Nd isotopes versus salinity in the modern deep Southern Ocean and Indian Ocean and the mixing relationship between NADW and CDW. Late Holocene authigenic Nd isotope data from SK129 (mean and 2σ for samples from ~3–6 ka) is also plotted with modern salinity at the site (estimated from Levitus94 at http://iridl.ldeo.columbia.edu). The seawater data are intended to be representative rather than exhaustive, with a focus on data from high quality recent data sets and water depths below ~2 km. The mixing line is between CDW in the Drake Passage ($\varepsilon_{Nd} = -8.5$; [Nd] = 24.2 pmol kg$^{-1}$; defined by data from depths of 2.5–3.5 km at stations 230, 236, 241, and 250 of *Stichel et al.* [2012]) and NADW in the northwest Atlantic ($\varepsilon_{Nd} = -13.2$; [Nd] = 21.2 pmol kg$^{-1}$; defined by data from depths of 1.8–4.0 km at station All 109–1 of *Piepgras and Wasserburg* [1987]). For clarity, measurement uncertainties are not shown on data points, but typical uncertainties are 0.3–0.4 $\varepsilon_{Nd}$ units and the maximum uncertainty is 0.5 $\varepsilon_{Nd}$ units. The dashed lines define a window that reflects this uncertainty, but we do not attempt to account for uncertainty in end-member Nd isotopic compositions or concentrations. Data sources are Drake Passage (stations 230, 236, 241, 250; 2.5–3.5 km) [*Stichel et al.*, 2012]; southeast Atlantic (42–53°S; stations 101, 104, 113; 2.0–4.4 km) [*Stichel et al.*, 2012]; Cape Basin (25°S; station 69/26; 2.0–4.8 km) [*Rickli et al.*, 2009]; southwest Pacific (multicores MuC-78 and MuC-79; 3.1–3.5 km) [*Molina-Kescher et al.*, 2014]; Bay of Bengal (stations 807–811; 2.0–3.6 km) [*Singh et al.*, 2012]; distal Bay of Bengal (station 806; 2.0–3.8 km) [*Singh et al.*, 2012]; and northwest Atlantic (stations TTO/TAS 63 and All 109–1; 1.8–4.0 km) [*Piepgras and Wasserburg*, 1987]. Three overlapping data points have been offset by a negligible amount in the *x* axis (0.005) to aid visualization.

deep Cape Basin (TNO57-21) and deep Indian Ocean (SK129) in the Holocene (Figure 5b) may be explained by the incorporation of a similar proportion of NADW into their water mass source regions in the mid-depths of the Southern Ocean. In addition, coincident changes in both SK129 and Cape Basin Nd isotope records over the last glacial cycle (Figure 5b) indicate similar NADW contributions at both sites through time, suggesting that a comparable connection existed between these sites in the past. That suggestion is also supported by the similarity of benthic $\delta^{18}O$ records from SK129 and the Cape Basin over the 0–250 ka interval (Figure 9), since this is a conservative tracer, although small differences in sourcing would be hard to resolve outside of the analytical and geological noise in $\delta^{18}O$ measurements.

### 6.2. Link Between Northern Hemisphere Climate and NADW Signature in the Indian Ocean

We suggest here that those Nd isotope changes in the Indian Ocean are recording a Northern Hemisphere climate signal, which is supported by three observations. First, there is a clear precessional signature in the SK129 Nd isotope record that is approximately in phase with Northern Hemisphere summer insolation maxima (Figures 6a and 7). Differences in the magnitude of the Nd isotope response between MIS 6.3 and MIS 6.5 further point towards a high-latitude control, because such amplitude modulation is a feature of high-latitude (but not low-latitude) summer insolation at these times. This precessional signature has not previously been observed in deep ocean circulation reconstructions based on Nd isotopes, which highlights the value of a high-resolution record that extends beyond the last glacial cycle. In particular, the last glacial period may have been quite unrepresentative because of the unusually weak precessional forcing at this time, which may also have allowed sub-orbital components of climate variability (e.g., Dansgaard-Oeschger and Heinrich events) to have played a more dominant role.

Second, the long-term sawtooth pattern in Nd isotopes resembles the characteristic pattern of sea level reconstructions from glacial cycles since the Mid-Pleistocene Transition, with slow ice sheet growth and rapid decay [e.g., *Bintanja et al.*, 2005; *Elderfield et al.*, 2012]. The indication here is of a close coupling between the Northern Hemisphere ice sheets, which largely control those sea level fluctuations, and deep ocean circulation.

Third, the Nd isotope record shows a striking similarity to grain size reconstructions from the Chinese Loess Plateau [*Yang and Ding*, 2014] (Figure 6b), which contain precessional variability superimposed on a glacial-interglacial sawtooth pattern. Those grain size records are interpreted in terms of the dynamics of the atmospheric circulation of the high-latitude Northern Hemisphere, and in particular the winter

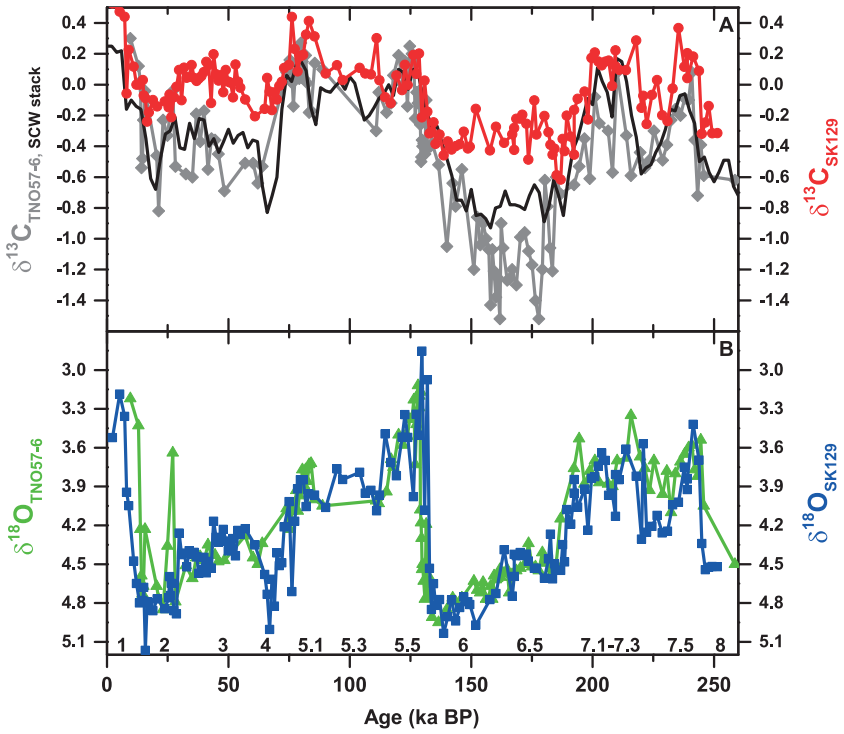


**Figure 9.** Comparison of (a) benthic $\delta^{13}C$ and (b) benthic $\delta^{18}O$ records between SK129 (this study) and the Cape Basin core TNO57-6 (43°S, 9°E, 3.75 km water depth) [*Hodell et al.*, 2000]. The TNO57-6 record is plotted on its original published age model. The benthic $\delta^{13}C$ record for the Southern Component Water stack [*Lisiecki*, 2010], for which TNO57-6 is one contributing record, is also shown (labeled SCW stack). Comparison of the benthic $\delta^{18}O$ records suggests similar water mass sourcing through time, as well as good stratigraphic alignment. Large differences in the $\delta^{13}C$ records may indicate that different transport pathways and/or timescales influenced the non-conservative behavior of this tracer. Numbers along the *x* axis are MIS numbers.

(northeast) monsoon strength in Asia [*Xiao et al.*, 1995; *Sun et al.*, 2006; *Yang and Ding*, 2014]. A stronger winter monsoon, producing a coarser grain size on the Chinese Loess Plateau, appears to correspond to more radiogenic Nd isotopes in SK129, indicating a reduced NADW signature in the Southern Ocean (Figure 6b). We conclude from these observations that there was a close coupling between those atmospheric and ocean circulation systems.

### 6.3. Mechanisms Controlling the NADW Signature in the Indian Ocean

We now consider in detail two possible mechanisms behind the changing NADW signature recorded at SK129 and a comparison to evidence for ocean circulation changes from other approaches.

#### 6.3.1. Changing NADW Export

The simplest explanation for our data may be to explicitly invoke changes in NADW production and export, as previously proposed to explain past Nd isotope variability in the Southern Ocean [*Piotrowski et al.*, 2005; *Robinson and van de Flierdt*, 2009; *Pena and Goldstein*, 2014], and also suggested in modeling studies for the Southern Ocean and Indian Ocean [*Rempfer et al.*, 2012; *Friedrich et al.*, 2014]. In this scenario, increased NADW export would coincide with interglacial periods and with precessional Northern Hemisphere insolation peaks within glacial periods (Figure 6a); it would also coincide with reduced ice sheet extent and weaker winter monsoon circulation in Asia (Figure 6b). The observed glacial-interglacial changes of up to 3 $\varepsilon_{Nd}$ units would appear to imply quite significant reductions in NADW export during glacial periods, although that reduction is hard to quantify due to potential changes in Nd isotopic compositions or Nd concentrations of the contributing water masses through time that are not fully constrained (see discussion in *Wilson et al.* [2014] and *Bohm et al.* [2015]).

Previous studies have also suggested a link between North Atlantic climate and changes in the Asian and Indian monsoonal circulations over a range of timescales [e.g., *Porter and An*, 1995; *Guo et al.*, 1998; *Marzin et al.*, 2013],

and some have invoked a role for changes in NADW formation [e.g., *Guo et al*., 1998; *Marzin et al*., 2013]. The new evidence from Nd isotopes in our study (Figure 6b), when combined with increased confidence in age models from the Chinese Loess Plateau [*Sun et al*., 2010], would appear to provide independent support for such a mechanism, now indicating a link on both orbital and glacial-interglacial timescales.

However, an in-phase response of Nd isotopes to Northern Hemisphere insolation that is mediated by changing NADW export appears to be inconsistent with other paleoceanographic evidence from the Late Pleistocene. In particular, inter-basin $\delta^{13}C$ gradients were interpreted as showing a significant lag of 6–11 kyr between Northern Hemisphere insolation in the precession band and NADW overturning [*Lisiecki et al*., 2008], almost opposite to the response inferred here. This discrepancy cannot simply reflect age model differences, because the chronology in both studies is tied to the same LR04 age scale. Therefore, we suggest that the discrepancy between these interpretations may reflect the significant challenge in making circulation reconstructions from carbon isotopes, due to the multiple controls on their oceanic distributions. For example, a recent modeling study [*Gebbie*, 2014] demonstrates that interpretations of carbon isotopes in terms of water mass variability even within the Atlantic Ocean may be impacted by non-conservative tracer behavior related to nutrient cycling in a non-analogue glacial ocean.

A qualitatively significant glacial reduction in NADW export also appears to indicate a discrepancy with evidence from North Atlantic Pa/Th reconstructions, because these data point to the continued production and relatively vigorous export of NADW, or a shallower equivalent Glacial North Atlantic Intermediate Water (GNAIW), within glacial periods [*Gherardi et al*., 2009], even at times when southern-sourced waters dominated the deep Atlantic [*Bohm et al*., 2015]. In light of potential controls on Pa/Th from particle scavenging behavior, in particular by opal [*Siddall et al*., 2005], we are quite cautious of interpreting those Pa/Th records in terms of NADW export [see also *Burke et al*., 2011]. Nevertheless, the apparent discrepancy between Nd isotopes and both $\delta^{13}C$ and Pa/Th evidence leads us to consider an alternative explanation for the observed Nd isotope changes.

#### 6.3.2. Changing Deep Ocean Structure

In our second scenario, we propose that the Nd isotopic composition of the deep Indian Ocean reflects the connectivity of the NADW overturning cell with the global deep oceans, rather than being related to NADW export or the strength of the Atlantic meridional overturning circulation. In the glacial circulation mode described by *Adkins* [2013] and *Ferrari et al*. [2014], the deep ocean would become isolated from an NADW source as the two-cell circulation structure developed [*Ferrari et al*., 2014, their Figure 4], with a distinct boundary at ~2–2.5 km water depth sustained by the restricted mixing between the two cells [*Lund et al*., 2011]. With the development of deep stratification during glacial periods [*Hodell et al*., 2003; *Lynch-Stieglitz et al*., 2007], the unradiogenic NADW signature could have been restricted to shallower depths of the Southern Ocean, allowing the deeper waters reaching SK129 to be more strongly influenced by the more radiogenic Nd isotope signature of recirculating Pacific waters.

The precession signature in our Nd isotope reconstruction may further support a control by Northern Hemisphere insolation, via the temperature of NADW, on deep stratification and mixing in the Southern Ocean, as proposed by *Adkins* [2013]. Obtaining reliable and well-dated sea ice reconstructions remains a major challenge, but sea-salt sodium records from Antarctic ice cores may provide such evidence and also contain a strong precession signal [*Wolff et al*., 2006]. That similarity may point towards the mechanism proposed by *Ferrari et al*. [2014] for a sea ice control on deep ocean structure, although we cannot determine whether NADW temperature or presence in the Southern Ocean is directly influencing Antarctic sea ice extent.

Studies of radiocarbon in deep-sea corals from the Drake Passage [*Burke and Robinson*, 2012] and in paired benthic and planktonic foraminifera from the deep South Atlantic [*Skinner et al*., 2010] also provide some insight into the glacial-interglacial evolution of the vertical structure of the Southern Ocean, although that evidence is limited to the last deglaciation. In general, these studies point towards the existence of large Southern Ocean vertical chemical gradients during the last glacial, which were also seen in South Atlantic and Southern Ocean benthic $\delta^{13}C$ records [*Hodell et al*., 2003]. *Skinner et al*. [2010] showed that Lower CDW was highly radiocarbon-depleted at the Last Glacial Maximum, potentially as a result of the deep recirculation of Pacific waters, whereas *Burke and Robinson* [2012] demonstrated a somewhat less dramatic reduction in the ventilation of Upper CDW between the Holocene and the Last Glacial Maximum. If the large glacial-interglacial changes in Nd isotopes recorded in SK129 were the result of increased Pacific

water recirculation into Upper CDW feeding the Indian Ocean during glacial periods, this scenario appears to require that the Pacific waters that contributed were also relatively well ventilated, which appears reasonable in light of radiocarbon evidence from the mid-depth Pacific Ocean [*Broecker et al*., 2008].

Resolving the extent to which our Nd isotope record is influenced by changes in NADW export from the Atlantic, versus changes in Southern Ocean water mass distributions, will require more extensive records from the intermediate and mid-depth Southern Ocean. It is also possible that these two mechanisms operated together, especially if some mixing between the two cells was still possible in the Southern Ocean during glacial periods, or if that water mass structure developed more gradually within glacial periods. However, at present, we consider changes in the deep ocean structure to be the predominant control, because that explanation is not inconsistent with the existing evidence from Pa/Th and $\delta^{13}C$ gradients, and because the link with Northern Hemisphere insolation and/or Antarctic sea ice changes appears to provide a viable explanation for the orbital signature. It is instructive to proceed on that basis and we explore some of the implications of our record for glacial carbon cycling and climate.

### 6.4. Role of Ocean Circulation in Glacial Inceptions

For the most recent glacial cycle, the onset of glacial conditions occurred in two major steps separated by ~45 kyr. An initial atmospheric $CO_2$ decrease of ~40 ppm occurred at the MIS 5.5–5.4 transition, with a subsequent decrease of ~30 ppm at the MIS 5–4 transition [*Luthi et al*., 2008]. Both changes were linked with significant Antarctic temperature changes as recorded in ice cores (Figure 5e), and attempts have been made to link this two-step process to particular mechanisms and processes occurring at different times [e.g., *Peacock et al*., 2006; *Hain et al*., 2010; *Sigman et al*., 2010].

From a Nd isotope perspective, the onset of the last glacial period (identified in terms of a significant shift in Nd isotopic composition at SK129) occurred at the MIS 5–4 transition rather than at the MIS 5.5–5.4 transition (Figure 5), coinciding with one of the precessional timescale changes in Nd isotopes (Figure 6a). In the South Atlantic sector of the Southern Ocean, enhanced vertical $\delta^{13}C$ gradients during glacial periods have been interpreted in terms of nutrient regeneration and carbon storage in a deep and potentially sluggish lower circulation cell [*Hodell et al*., 2003], a structure that also emerged at the MIS 5–4 transition. Whereas vertical $\delta^{13}C$ gradients are influenced by biogeochemical cycling, Nd isotopes are responding to circulation changes alone. The coincidence of these changes therefore supports an active role for changing ocean circulation in the carbon storage at these times, consistent with the hypothesis that cooling NADW and/or increasing Antarctic sea ice extent would lead to increased deep stratification and isolation of the deep Southern Ocean [*Adkins*, 2013]. A similar pattern and timing of changes in Nd isotopes and South Atlantic vertical $\delta^{13}C$ gradients is also observed for the previous glacial inception at the MIS 7–6 boundary (Figure 6a), suggesting that precession may play an important role in the timing of glacial inceptions.

Focusing on the atmospheric $CO_2$ changes accompanying the most recent glacial inception, our Nd isotope evidence appears to rule out a role for changing deep ocean circulation structure in the $CO_2$ decrease at the MIS 5.5–5.4 transition. This initial decline therefore requires an alternative mechanism; for example, polar Antarctic stratification accompanied by some whole ocean cooling [*Hain et al*., 2010; *Sigman et al*., 2010]. In contrast, our data support a role for ocean circulation reorganization in the later decline in $CO_2$ at the MIS 5–4 transition. For example, *Hain et al*. [2010] propose that a circulation change involving an NADW-GNAIW switch in combination with the aforementioned changes in the Antarctic could have played a role in the glacial atmospheric $CO_2$ decrease. Our Nd isotope data, if interpreted in terms of changes in deep ocean structure, suggest that this NADW-GNAIW circulation switch could have occurred at the MIS 5–4 transition but not before, which is also in agreement with the timing suggested by *Adkins* [2013] for the onset of deep stratification based on Atlantic Ocean cooling.

### 6.5. Decoupled Ocean Circulation and Carbon Cycling During Glacial Periods

In contrast to the generally coupled changes in Nd isotopes and $\delta^{13}C$ during glacial inception and deglaciation, the evolution of these tracers was decoupled at other times in our record, particularly during glacial periods (Figure 6c). The decoupling argues against a simple interpretation of the $\delta^{13}C$ record in terms of water mass mixing. Unlike the sawtooth shape of the Nd isotope record, which we have linked to a Northern Hemisphere control (Figure 6b), the square wave form of the SK129 $\delta^{13}C$ record is more similar

to the evolution of Antarctic temperature (Figure 6d), with finer-scale similarities also on sub-orbital timescales. Although an offset in this graphical comparison emerges across multiple glacial cycles (Figure 6d), this feature may be readily linked to a long-term increasing global trend in $\delta^{13}C$ [*Wang et al*., 2004; *Hoogakker et al*., 2006].

Based on the overall similarity between Antarctic temperature and $\delta^{13}C$, we suggest a southern origin for the $\delta^{13}C$ signal, which would be consistent with a dominant Southern Ocean control on glacial climates, such as through changes in nutrient utilization [e.g., *Sigman et al*., 2010]. In addition to changes in preformed nutrient contents in the deep water source regions, the $\delta^{13}C$ record may also have been influenced by changes in air-sea exchange in those regions, changes in nutrient regeneration at depth, or changes in the nutrient content of Pacific waters mixed into the Southern Ocean.

Given these multiple controls on the $\delta^{13}C$ record, there is a clear difficulty in providing a unique interpretation, and we instead emphasize two key points. First, the similarity of $\delta^{13}C$ with Antarctic climate, together with differences from Nd isotopes, suggests that carbon isotopes within CDW are strongly reset by biogeochemical processes in the Southern Ocean. It is important to emphasize that the Nd isotope record relates to mixing between distinct Atlantic and Pacific end-members but does not constrain ventilation processes occurring in the Southern Ocean since these may occur without a significant change in Nd isotopes. Therefore, a strong Southern Hemisphere climate signature in the $\delta^{13}C$ record can be distinguished even while Nd isotopes carry a Northern Hemisphere signature. Second, while both Nd isotopes and benthic $\delta^{18}O$ point to similar water mass sourcing to the deep Central Indian Ocean and the deep Cape Basin through time (Figures 5b and 9b), their benthic $\delta^{13}C$ records diverge strongly during glacial periods (Figure 9a), indicating differences in carbon cycling between these regions. One possible interpretation is that these locations were influenced by the same mixture of water masses through time, but that very different transport pathways and/or timescales influenced the non-conservative behavior of the $\delta^{13}C$ tracer, with a sluggish circulation in the deep southeast Atlantic Ocean allowing a large reservoir of respired nutrients to build up.

Perhaps the clearest example of decoupling between the two tracers emerges during the MIS 6.5 substage, when Nd isotopes indicate a large NADW component at SK129 (Figure 5b), similar to interglacial periods, while $\delta^{13}C$ values were close to glacial values (Figure 5c), along with Antarctic temperature (Figure 5e) and atmospheric $CO_2$ [*Luthi et al*., 2008]. One possibility is that warmer substages of glacial periods were associated with a weaker deep stratification and greater mixing between the two cells globally. Alternatively, the Indian Ocean may have been more directly connected to the Atlantic Ocean at these times, perhaps similar to today, but that may not have been representative of the global deep ocean. In either case, it appears that such mid-depth water mass source changes did not significantly influence the Southern Ocean carbon cycle during glacial periods. For example, atmospheric $CO_2$ (although quite poorly resolved) does not appear to have risen by any more than 20 ppm at this time [*Luthi et al*., 2008]. That sets a limit on the effect of such a circulation change on atmospheric $CO_2$, and one that seems fairly reasonable in light of modeling studies [e.g., *Hain et al*., 2010]. The further implication is that while decreasing NADW temperature or presence in the Southern Ocean may help to initiate a glacial period, increasing NADW temperature or presence during a glacial period may not in itself lead to deglaciation, i.e., once glacial boundary conditions have been established, such a mechanism does not appear to be reversible in any simple manner.

Combining Nd isotope and $\delta^{13}C$ tracers has led to improved insights on the carbon cycle, but benthic $\delta^{13}C$ does not constrain deep ocean carbon storage in a simple way; for example, being sensitive also to the evolving partitioning of carbon between the atmosphere and biosphere. Therefore, a fuller understanding of the links between ocean circulation, biogeochemistry, and oceanic carbon storage could potentially be obtained by integrating such records with evidence on the deep ocean carbonate system [e.g., *Yu et al*., 2010].

### 6.6. Long-Term Feedback Between Ice Sheets and Ocean Circulation

On timescales longer than orbital precession, Nd isotopes in SK129 record a long-term sawtooth trend within glacial periods that differs from both benthic $\delta^{13}C$ (Figure 6c) and Antarctic climate (Figure 5). Similar features are also observed in deep ocean Nd isotope records from the Cape Basin [*Piotrowski et al*., 2008] and Bermuda Rise [*Bohm et al*., 2015], suggesting that this observation is robust. Although changes over such a long timescale are hard to unequivocally equate to their forcing, we suggest that this signature may indicate a

gradual reduction in NADW formation and export into the Southern Ocean through glacial periods. The slow growth of Northern Hemisphere ice sheets may have been responsible because of the associated changes in freshwater fluxes, sea ice extent, and atmospheric circulation. Therefore, while Southern Ocean processes appear to have controlled the glacial carbon cycle, declining NADW may have provided an additional positive feedback on glacial climate linked to the Northern Hemisphere.

An alternative explanation for the sawtooth pattern might call upon glacial weathering changes to influence Nd inputs and water mass end-members in the high-latitude North Atlantic [e.g., *von Blanckenburg and Nagler*, 2001]. It is at least conceivable that such a process could explain a link between sea level (i.e., ice sheet volume) and Nd isotopes. However, that possibility is poorly constrained at present, whereas we note that a relatively gradual transition towards a full glacial circulation pattern has been documented in a range of other proxy records [*Martinez-Mendez et al*., 2008; *Alonso-Garcia et al*., 2011; *Bohm et al*., 2015]. Therefore, we emphasize that the deep ocean circulation structure at glacial maxima, and the starting point for the ensuing terminations, may have been different from that during earlier stages of glaciation.

## 7. Conclusions

We have used multiple authigenic phases in sediment core SK129-CR2 to reconstruct the Nd isotope evolution of CDW in the deep Indian Ocean through the last two glacial cycles (0–250 ka B.P.). Despite potential challenges with the reliability of data from sediment leachates, we have demonstrated that a robust reconstruction is achievable. By comparing Nd isotope evidence on water mass sourcing to the carbon isotope evolution in the same core, and to other global climate records, we have investigated the role of ocean circulation change in glacial cycles and the potential orbital controls influencing that ocean-climate link.

Our evidence indicates that Northern Hemisphere and Southern Hemisphere processes exerted a combined influence on the water mass structure and carbon chemistry of the deep ocean through multiple glacial-interglacial cycles. Seawater Nd isotopes record the changing influence of NADW in the Southern Ocean, which responded to both direct orbital forcing in the precession band and to glacial amplification through glacial cycles. The orbital timescale changes could suggest an active role for ocean circulation changes driven from the Northern Hemisphere in initiating glacial climates, possibly through the effect of cooling NADW on the deep stratification and carbon storage capacity of the glacial Southern Ocean. In contrast, within glacial periods, mid-depth water mass mixing and deep ocean carbon storage were apparently decoupled, with MIS 6.5 providing a striking example that warrants further study. Once glacial conditions were established, Southern Ocean processes appear to have played the dominant role in the ocean's carbon cycle. Nevertheless, a gradual reduction of NADW within glacial periods could have been linked to the slow growth of Northern Hemisphere ice sheets and related atmospheric circulation change, potentially providing an additional climate feedback as the Earth evolved towards its glacial maxima.

**Acknowledgments**

Data to support this article are provided in Tables S1–S6 of the supporting information. We thank Jo Clegg, Jason Day, Linda Booth, Mike Hall, and James Rolfe for laboratory support, and Harry Elderfield for helpful comments on an earlier version of the manuscript. We are also grateful to Jimin Yu, Chris Charles, and anonymous reviewers for their detailed comments and suggestions that helped us to improve the manuscript. This study was supported by a NERC studentship to D.J.W. and NERC grant NE/F006047/1, RG50124 to A.M.P./A.G.

## References

Adkins, J. F. (2013), The role of deep ocean circulation in setting glacial climates, *Paleoceanography*, *28*, 539–561, doi:10.1002/palo.20046.

Albarede, F., S. L. Goldstein, and D. Dautel (1997), The neodymium isotopic composition of manganese nodules from the Southern and Indian oceans, the global oceanic neodymium budget, and their bearing on deep ocean circulation, *Geochim. Cosmochim. Acta*, *61*(6), 1277–1291.

Alonso-Garcia, M., F. J. Sierro, M. Kucera, J. A. Flores, I. Cacho, and N. Andersen (2011), Ocean circulation, ice sheet growth and interhemispheric coupling of millennial climate variability during the mid-Pleistocene (ca 800–400 ka), *Quat. Sci. Rev.*, *30*(23–24), 3234–3247.

Anderson, R. F., S. Ali, L. I. Bradtmiller, S. H. H. Nielsen, M. Q. Fleisher, B. E. Anderson, and L. H. Burckle (2009), Wind-driven upwelling in the Southern Ocean and the deglacial rise in atmospheric $CO_2$, *Science*, *323*(5920), 1443–1448.

Banakar, V. K. (2005), $\delta^{13}C$ depleted oceans before the Termination 2: More nutrient-rich deep-water formation or light-carbon transfer?, *Indian J. Mar. Sci.*, *34*(3), 249–258.

Bayon, G., C. R. German, R. M. Boella, J. A. Milton, R. N. Taylor, and R. W. Nesbitt (2002), An improved method for extracting marine sediment fractions and its application to Sr and Nd isotopic analysis, *Chem. Geol.*, *187*(3–4), 179–199.

Berger, A., and M. F. Loutre (1991), Insolation values for the climate of the last 10 million years, *Quat. Sci. Rev.*, *10*(4), 297–317.

Bintanja, R., R. S. W. van de Wal, and J. Oerlemans (2005), Modelled atmospheric temperatures and global sea levels over the past million years, *Nature*, *437*(7055), 125–128.

Bohm, E., J. Lippold, M. Gutjahr, M. Frank, P. Blaser, B. Antz, J. Fohlmeister, N. Frank, M. B. Andersen, and M. Deininger (2015), Strong and deep Atlantic meridional overturning circulation during the last glacial cycle, *Nature*, *517*(7532), 73–76.

Boyle, E. A., and L. D. Keigwin (1985), Comparison of Atlantic and Pacific paleochemical records for the last 215,000 years: Changes in deep ocean circulation and chemical inventories, *Earth Planet. Sci. Lett.*, *76*(1–2), 135–150.

Broecker, W., E. Clark, and S. Barker (2008), Near constancy of the Pacific Ocean surface to mid-depth radiocarbon-age difference over the last 20 kyr, *Earth Planet. Sci. Lett.*, *274*(3–4), 322–326.

Broecker, W. S., and G. H. Denton (1989), The role of ocean–atmosphere reorganizations in glacial cycles, *Geochim. Cosmochim. Acta*, *53*(10), 2465–2501.
Burke, A., and L. F. Robinson (2012), The Southern Ocean's role in carbon exchange during the last deglaciation, *Science*, *335*(6068), 557–561.
Burke, A., O. Marchal, L. I. Bradtmiller, J. F. McManus, and R. Francois (2011), Application of an inverse method to interpret $^{231}$Pa/$^{230}$Th observations from marine sediments, *Paleoceanography*, *26*, PA1212, doi:10.1029/2010PA002022.
Carter, P., D. Vance, C. D. Hillenbrand, J. A. Smith, and D. R. Shoosmith (2012), The neodymium isotopic composition of waters masses in the eastern Pacific sector of the Southern Ocean, *Geochim. Cosmochim. Acta*, *79*, 41–59.
Chester, R., and M. J. Hughes (1967), A chemical technique for the separation of ferro-manganese minerals, carbonate minerals and adsorbed trace elements from pelagic sediments, *Chem. Geol.*, *2*, 249–262.
Colin, C., L. Turpin, J. Bertaux, A. Desprairies, and C. Kissel (1999), Erosional history of the Himalayan and Burman ranges during the last two glacial-interglacial cycles, *Earth Planet. Sci. Lett.*, *171*(4), 647–660.
Drysdale, R. N., J. C. Hellstrom, G. Zanchetta, A. E. Fallick, M. F. S. Goni, I. Couchoud, J. McDonald, R. Maas, G. Lohmann, and I. Isola (2009), Evidence for obliquity forcing of Glacial Termination II, *Science*, *325*(5947), 1527–1531.
Elderfield, H., P. Ferretti, M. Greaves, S. Crowhurst, I. N. McCave, D. Hodell, and A. M. Piotrowski (2012), Evolution of ocean temperature and ice volume through the Mid-Pleistocene Climate Transition, *Science*, *337*(6095), 704–709.
Ferrari, R., M. F. Jansen, J. F. Adkins, A. Burke, A. L. Stewart, and A. F. Thompson (2014), Antarctic sea ice control on ocean circulation in present and glacial climates, *Proc. Natl. Acad. Sci. U.S.A.*, *111*(24), 8753–8758.
Frank, M. (2002), Radiogenic isotopes: Tracers of past ocean circulation and erosional input, *Rev. Geophys.*, *40*(1), 1001, doi:10.1029/2000RG000094.
Friedrich, T., A. Timmermann, T. Stichel, and K. Pahnke (2014), Ocean circulation reconstructions from $\varepsilon_{Nd}$: A model-based feasibility study, *Paleoceanography*, *29*, 1003–1023, doi:10.1002/2014PA002658.
Ganachaud, A., C. Wunsch, J. Marotzke, and J. Toole (2000), Meridional overturning and large-scale circulation of the Indian Ocean, *J. Geophys. Res.*, *105*(C11), 26,117–26,134, doi:10.1029/2000JC900122.
Gebbie, G. (2014), How much did Glacial North Atlantic Water shoal?, *Paleoceanography*, *29*, 190–209, doi:10.1002/2013PA002557.
Gherardi, J. M., L. Labeyrie, S. Nave, R. Francois, J. F. McManus, and E. Cortijo (2009), Glacial-interglacial circulation changes inferred from $^{231}$Pa/$^{230}$Th sedimentary record in the North Atlantic region, *Paleoceanography*, *24*, PA2204, doi:10.1029/2008PA001696.
Goldstein, S. L., and S. R. Hemming (2003), Long-lived isotopic tracers in oceanography, paleoceanography and ice sheet dynamics, in *The Oceans and Marine Geochemistry*, edited by H. Elderfield, pp. 453–489, Elsevier-Pergamon, Oxford, U. K.
Goswami, V., S. K. Singh, and R. Bhushan (2014), Impact of water mass mixing and dust deposition on Nd concentration and $\varepsilon_{Nd}$ of the Arabian Sea water column, *Geochim. Cosmochim. Acta*, *145*, 30–49.
Gourlan, A. T., L. Meynadier, C. J. Allegre, P. Tapponnier, J. L. Birck, and J. L. Joron (2010), Northern Hemisphere climate control of the Bengali rivers discharge during the past 4 Ma, *Quat. Sci. Rev.*, *29*(19–20), 2484–2498.
Guo, Z. T., T. S. Liu, N. Fedoroff, L. Y. Wei, Z. L. Ding, N. Q. Wu, H. Y. Lu, W. Y. Jiang, and Z. S. An (1998), Climate extremes in Loess of China coupled with the strength of deep-water formation in the North Atlantic, *Global Planet. Change*, *18*(3–4), 113–128.
Gutjahr, M., M. Frank, C. H. Stirling, V. Klemm, T. van de Flierdt, and A. N. Halliday (2007), Reliable extraction of a deepwater trace metal isotope signal from Fe-Mn oxyhydroxide coatings of marine sediments, *Chem. Geol.*, *242*(3–4), 351–370.
Hain, M. P., D. M. Sigman, and G. H. Haug (2010), Carbon dioxide effects of Antarctic stratification, North Atlantic Intermediate Water formation, and subantarctic nutrient drawdown during the last ice age: Diagnosis and synthesis in a geochemical box model, *Global Biogeochem. Cycles*, *24*, GB4023, doi:10.1029/2010GB003790.
Hall, I. R., I. N. McCave, N. J. Shackleton, G. P. Weedon, and S. E. Harris (2001), Intensified deep Pacific inflow and ventilation in Pleistocene glacial times, *Nature*, *412*(6849), 809–812.
Heinze, C., I. Kriest, and E. Maier-Reimer (2009), Age offsets among different biogenic and lithogenic components of sediment cores revealed by numerical modeling, *Paleoceanography*, *24*, PA4214, doi:10.1029/2008PA001662.
Hodell, D. A., C. D. Charles, and U. S. Ninnemann (2000), Comparison of interglacial stages in the South Atlantic sector of the southern ocean for the past 450 kyr: Implifications for marine isotope stage (MIS) 11, *Global Planet. Change*, *24*(1), 7–26.
Hodell, D. A., K. A. Venz, C. D. Charles, and U. S. Ninnemann (2003), Pleistocene vertical carbon isotope and carbonate gradients in the South Atlantic sector of the Southern Ocean, *Geochem. Geophys. Geosyst.*, *4*(1), 1004, doi:10.1029/2002GC000367.
Hoogakker, B. A. A., E. J. Rohling, M. R. Palmer, T. Tyrrell, and R. G. Rothwell (2006), Underlying causes for long-term global ocean $\delta^{13}$C fluctuations over the last 1.20 Myr, *Earth Planet. Sci. Lett.*, *248*(1–2), 15–29.
Imbrie, J., et al. (1992), On the structure and origin of major glaciation cycles 1. Linear responses to Milankovitch forcing, *Paleoceanography*, *7*(6), 701–738, doi:10.1029/92PA02253.
Jacobsen, S. B., and G. J. Wasserburg (1980), Sm-Nd isotopic composition of chondrites, *Earth Planet. Sci. Lett.*, *50*(1), 139–155.
Lisiecki, L. E. (2010), A simple mixing explanation for late Pleistocene changes in the Pacific-South Atlantic benthic $\delta^{13}$C gradient, *Clim. Past.*, *6*(3), 305–314.
Lisiecki, L. E., and M. E. Raymo (2005), A Pliocene-Pleistocene stack of 57 globally distributed benthic $\delta^{18}$O records, *Paleoceanography*, *20*, PA1003, doi:10.1029/2004PA001071.
Lisiecki, L. E., and M. E. Raymo (2009), Diachronous benthic $\delta^{18}$O responses during late Pleistocene terminations, *Paleoceanography*, *24*, PA3210, doi:10.1029/2009PA001732.
Lisiecki, L. E., M. E. Raymo, and W. B. Curry (2008), Atlantic overturning responses to Late Pleistocene climate forcings, *Nature*, *456*(7218), 85–88.
Lund, D. C., J. F. Adkins, and R. Ferrari (2011), Abyssal Atlantic circulation during the Last Glacial Maximum: Constraining the ratio between transport and vertical mixing, *Paleoceanography*, *26*, PA1213, doi:10.1029/2010PA001938.
Lupker, M., C. France-Lanord, V. Galy, J. Lave, and H. Kudrass (2013), Increasing chemical weathering in the Himalayan system since the Last Glacial Maximum, *Earth Planet. Sci. Lett.*, *365*, 243–252.
Luthi, D., et al. (2008), High-resolution carbon dioxide concentration record 650,000-800,000 years before present, *Nature*, *453*(7193), 379–382.
Lynch-Stieglitz, J., et al. (2007), Atlantic meridional overturning circulation during the Last Glacial Maximum, *Science*, *316*(5821), 66–69.
Mantyla, A. W., and J. L. Reid (1995), On the origins of deep and bottom waters of the Indian Ocean, *J. Geophys. Res.*, *100*(C2), 2417–2439, doi:10.1029/94JC02564.
Martin, E. E., and B. A. Haley (2000), Fossil fish teeth as proxies for seawater Sr and Nd isotopes, *Geochim. Cosmochim. Acta*, *64*(5), 835–847.
Martin, E. E., S. W. Blair, G. D. Kamenov, H. D. Scher, E. Bourbon, C. Basak, and D. N. Newkirk (2010), Extraction of Nd isotopes from bulk deep sea sediments for paleoceanographic studies on Cenozoic time scales, *Chem. Geol.*, *269*(3–4), 414–431.
Martinez-Mendez, G., R. Zahn, I. R. Hall, L. D. Pena, and I. Cacho (2008), 345,000-year-long multi-proxy records off South Africa document variable contributions of northern versus southern component water to the deep South Atlantic, *Earth Planet. Sci. Lett.*, *267*(1–2), 309–321.

Martinson, D. G., N. G. Pisias, J. D. Hays, J. Imbrie, T. C. Moore, and N. J. Shackleton (1987), Age dating and the orbital theory of the Ice Ages: development of a high-resolution 0 to 300,000-year chronostratigraphy, *Quat. Res.*, *27*(1), 1–29.
Marzin, C., N. Kallel, M. Kageyama, J. C. Duplessy, and P. Braconnot (2013), Glacial fluctuations of the Indian monsoon and their relationship with North Atlantic climate: New data and modelling experiments, *Clim. Past.*, *9*(5), 2135–2151.
McCave, I. N., T. Kiefer, D. J. R. Thornalley, and H. Elderfield (2005), Deep flow in the Madagascar-Mascarene Basin over the last 150 000 years, *Philos. Trans. R. Soc. London, Ser. A*, *363*(1826), 81–99.
Miller, M. D., J. F. Adkins, D. Menemenlis, and M. P. Schodlok (2012), The role of ocean cooling in setting glacial southern source bottom water salinity, *Paleoceanography*, *27*, PA3207, doi:10.1029/2012PA002297.
Molina-Kescher, M., M. Frank, and E. Hathorne (2014), South Pacific dissolved Nd isotope compositions and rare earth element distributions: Water mass mixing versus biogeochemical cycling, *Geochim. Cosmochim. Acta*, *127*, 171–189.
Palmer, M. R., and H. Elderfield (1985), Variations in the Nd isotopic composition of foraminifera from Atlantic Ocean sediments, *Earth Planet. Sci. Lett.*, *73*(2–4), 299–305.
Peacock, S., E. Lane, and J. M. Restrepo (2006), A possible sequence of events for the generalized glacial-interglacial cycle, *Global Biogeochem. Cycles*, *20*, GB2010, doi:10.1029/2005GB002448.
Pena, L. D., and S. L. Goldstein (2014), Thermohaline circulation crisis and impacts during the mid-Pleistocene transition, *Science*, *345*(6194), 318–322.
Petit, J. R., et al. (1999), Climate and atmospheric history of the past 420,000 years from the Vostok ice core, Antarctica, *Nature*, *399*(6735), 429–436.
Piepgras, D. J., and G. J. Wasserburg (1987), Rare earth element transport in the western North Atlantic inferred from Nd isotopic observations, *Geochim. Cosmochim. Acta*, *51*(5), 1257–1271.
Piotrowski, A. M., S. L. Goldstein, S. R. Hemming, and R. G. Fairbanks (2005), Temporal relationships of carbon cycling and ocean circulation at glacial boundaries, *Science*, *307*(5717), 1933–1938.
Piotrowski, A. M., S. L. Goldstein, S. R. Hemming, R. G. Fairbanks, and D. R. Zylberberg (2008), Oscillating glacial northern and southern deep water formation from combined neodymium and carbon isotopes, *Earth Planet. Sci. Lett.*, *272*(1–2), 394–405.
Piotrowski, A. M., V. K. Banakar, A. E. Scrivner, H. Elderfield, A. Galy, and A. Dennis (2009), Indian Ocean circulation and productivity during the last glacial cycle, *Earth Planet. Sci. Lett.*, *285*(1–2), 179–189.
Piotrowski, A. M., A. Galy, J. A. L. Nicholl, N. Roberts, D. J. Wilson, J. A. Clegg, and J. Yu (2012), Reconstructing deglacial North and South Atlantic deep water sourcing using foraminiferal Nd isotopes, *Earth Planet. Sci. Lett.*, *357*, 289–297.
Porter, S. C., and Z. S. An (1995), Correlation between climate events in the North Atlantic and China during the last glaciation, *Nature*, *375*(6529), 305–308.
Rempfer, J., T. F. Stocker, F. Joos, J. C. Dutay, and M. Siddall (2011), Modelling Nd-isotopes with a coarse resolution ocean circulation model: Sensitivities to model parameters and source/sink distributions, *Geochim. Cosmochim. Acta*, *75*(20), 5927–5950.
Rempfer, J., T. F. Stocker, F. Joos, and J. C. Dutay (2012), On the relationship between Nd isotopic composition and ocean overturning circulation in idealized freshwater discharge events, *Paleoceanography*, *27*, PA3211, doi:10.1029/2012PA002312.
Rickli, J., M. Frank, and A. N. Halliday (2009), The hafnium-neodymium isotopic composition of Atlantic seawater, *Earth Planet. Sci. Lett.*, *280*(1–4), 118–127.
Rickli, J., M. Gutjahr, D. Vance, M. Fischer-Goedde, C. D. Hillenbrand, and G. Kuhn (2014), Neodymium and hafnium boundary contributions to seawater along the West Antarctic continental margin, *Earth Planet. Sci. Lett.*, *394*, 99–110.
Roberts, N. L., A. M. Piotrowski, J. F. McManus, and L. D. Keigwin (2010), Synchronous deglacial overturning and water mass source changes, *Science*, *327*(5961), 75–78.
Roberts, N. L., A. M. Piotrowski, H. Elderfield, T. I. Eglinton, and M. W. Lomas (2012), Rare earth element association with foraminifera, *Geochim. Cosmochim. Acta*, *94*, 57–71.
Robinson, L. F., and T. van de Flierdt (2009), Southern Ocean evidence for reduced export of North Atlantic Deep Water during Heinrich event 1, *Geology*, *37*(3), 195–198.
Siddall, M., G. M. Henderson, N. R. Edwards, M. Frank, S. A. Muller, T. F. Stocker, and F. Joos (2005), $^{231}$Pa/$^{230}$Th fractionation by ocean transport, biogenic particle flux and particle type, *Earth Planet. Sci. Lett.*, *237*(1–2), 135–155.
Siddall, M., S. Khatiwala, T. van de Flierdt, K. Jones, S. L. Goldstein, S. Hemming, and R. F. Anderson (2008), Towards explaining the Nd paradox using reversible scavenging in an ocean general circulation model, *Earth Planet. Sci. Lett.*, *274*(3–4), 448–461.
Sigman, D. M., M. P. Hain, and G. H. Haug (2010), The polar ocean and glacial cycles in atmospheric $CO_2$ concentration, *Nature*, *466*(7302), 47–55.
Singh, S. P., S. K. Singh, V. Goswami, R. Bhushan, and V. K. Rai (2012), Spatial distribution of dissolved neodymium and $\varepsilon_{Nd}$ in the Bay of Bengal: Role of particulate matter and mixing of water masses, *Geochim. Cosmochim. Acta*, *94*, 38–56.
Skinner, L. C., and N. J. Shackleton (2005), An Atlantic lead over Pacific deep-water change across Termination I: implications for the application of the marine isotope stage stratigraphy, *Quat. Sci. Rev.*, *24*(5–6), 571–580.
Skinner, L. C., S. Fallon, C. Waelbroeck, E. Michel, and S. Barker (2010), Ventilation of the deep Southern Ocean and deglacial $CO_2$ rise, *Science*, *328*(5982), 1147–1151.
Staudigel, H., P. Doyle, and A. Zindler (1985), Sr and Nd isotope systematics in fish teeth, *Earth Planet. Sci. Lett.*, *76*(1–2), 45–56.
Stichel, T., M. Frank, J. Rickli, and B. A. Haley (2012), The hafnium and neodymium isotope composition of seawater in the Atlantic sector of the Southern Ocean, *Earth Planet. Sci. Lett.*, *317*, 282–294.
Sun, Y., J. Chen, S. C. Clemens, Q. S. Liu, J. F. Ji, and R. Tada (2006), East Asian monsoon variability over the last seven glacial cycles recorded by a loess sequence from the northwestern Chinese Loess Plateau, *Geochem. Geophys. Geosyst.*, *7* Q12Q02, doi:10.1029/2006GC001287.
Sun, Y. B., X. L. Wang, Q. S. Liu, and S. C. Clemens (2010), Impacts of post-depositional processes on rapid monsoon signals recorded by the last glacial loess deposits of northern China, *Earth Planet. Sci. Lett.*, *289*(1–2), 171–179.
Tachikawa, K., A. M. Piotrowski, and G. Bayon (2014), Neodymium associated with foraminiferal carbonate as a recorder of seawater isotopic signatures, *Quat. Sci. Rev.*, *88*, 1–13.
Tagliabue, A., L. Bopp, D. M. Roche, N. Bouttes, J. C. Dutay, R. Alkama, M. Kageyama, E. Michel, and D. Paillard (2009), Quantifying the roles of ocean circulation and biogeochemistry in governing ocean carbon-13 and atmospheric carbon dioxide at the last glacial maximum, *Clim. Past.*, *5*(4), 695–706.
Tanaka, T., et al. (2000), JNdi-1: A neodymium isotopic reference in consistency with LaJolla neodymium, *Chem. Geol.*, *168*(3–4), 279–281.
Toggweiler, J. R. (1999), Variation of atmospheric $CO_2$ by ventilation of the ocean's deepest water, *Paleoceanography*, *14*(5), 571–588, doi:10.1029/1999PA900033.
Toggweiler, J. R., J. L. Russell, and S. R. Carson (2006), Midlatitude westerlies, atmospheric $CO_2$, and climate change during the ice ages, *Paleoceanography*, *21*, PA2005, doi:10.1029/2005PA001154.

Torrence, C., and G. P. Compo (1998), A practical guide to wavelet analysis, *Bull. Am. Meteorol. Soc.*, *79*(1), 61–78.
von Blanckenburg, F., and T. F. Nagler (2001), Weathering versus circulation-controlled changes in radiogenic isotope tracer composition of the Labrador Sea and North Atlantic Deep Water, *Paleoceanography*, *16*(4), 424–434, doi:10.1029/2000PA000550.
Wang, P. X., J. Tian, X. R. Cheng, C. L. Liu, and J. Xu (2004), Major Pleistocene stages in a carbon perspective: The South China Sea record and its global comparison, *Paleoceanography*, *19*, PA4005, doi:10.1029/2003PA000991.
Wasserburg, G. J., S. B. Jacobsen, D. J. Depaolo, M. T. McCulloch, and T. Wen (1981), Precise determination of Sm/Nd ratios, Sm and Nd isotopic abundances in standard solutions, *Geochim. Cosmochim. Acta*, *45*(12), 2311–2323.
Wilson, D. J., A. M. Piotrowski, A. Galy, and J. A. Clegg (2013), Reactivity of neodymium carriers in deep sea sediments: Implications for boundary exchange and paleoceanography, *Geochim. Cosmochim. Acta*, *109*, 197–221.
Wilson, D. J., K. C. Crocket, T. van de Flierdt, L. F. Robinson, and J. F. Adkins (2014), Dynamic intermediate ocean circulation in the North Atlantic during Heinrich Stadial 1: A radiocarbon and neodymium isotope perspective, *Paleoceanography*, *29*, 1072–1093, doi:10.1002/2014PA002674.
Wolff, E. W., et al. (2006), Southern Ocean sea-ice extent, productivity and iron flux over the past eight glacial cycles, *Nature*, *440*(7083), 491–496.
Xiao, J., S. C. Porter, Z. S. An, H. Kumai, and S. Yoshikawa (1995), Grain size of quartz as an indicator of winter monsoon strength on the Loess Plateau of Central China during the last 130,000 yr, *Quat. Res.*, *43*(1), 22–29.
Yang, S., and Z. Ding (2014), A 249 kyr stack of eight loess grain size records from northern China documenting millennial-scale climate variability, *Geochem. Geophys. Geosyst.*, *15*, 798–814, doi:10.1002/2013GC005113.
You, Y. (2000), Implications of the deep circulation and ventilation of the Indian Ocean on the renewal mechanism of North Atlantic Deep Water, *J. Geophys. Res.*, *105*(C10), 23,895–23,926, doi:10.1029/2000JC900105.
Yu, J. M., W. S. Broecker, H. Elderfield, Z. D. Jin, J. McManus, and F. Zhang (2010), Loss of carbon from the deep sea since the Last Glacial Maximum, *Science*, *30*(6007), 1084–1087.

*Paleoceanography*

Supporting Information for

# Interhemispheric controls on deep ocean circulation and carbon chemistry during the last two glacial cycles

David J. Wilson[1,2*]
Alexander M. Piotrowski[1]
Albert Galy[1,3]
Virupaxa K. Banakar[4]

1 - Godwin Laboratory for Palaeoclimate Research, Department of Earth Sciences, University of Cambridge, Cambridge, CB2 3EQ, UK.

2 - Department of Earth Science and Engineering, Imperial College London, London, SW7 2AZ, UK.

3 - CRPG, Université de Lorraine, CNRS, 15 rue Notre Dame des Pauvres, BP 20, 54501 Vandoeuvre-lès-Nancy, France.

4 - National Institute of Oceanography, Dona Paula, Goa, 403 004, India.

* Corresponding author: david.wilson1@imperial.ac.uk

## Contents

## Introduction

This data set contains Nd isotope measurements made on acid-reductive sediment leachates, uncleaned planktonic foraminifera and fish teeth from core SK129-CR2 in the Central Indian Ocean spanning approximately 0-250 ka BP. It also includes benthic $\delta^{13}C$ and $\delta^{18}O$ data measured on the benthic foraminifera *Cibicidoides wuellerstorfi* in that core and age model information.

The Nd isotope data were collected on a Nu Plasma MC-ICP-MS at the University of Cambridge. The benthic $\delta^{13}C$ and $\delta^{18}O$ data were collected on a VG SIRA or a VG PRISM mass spectrometer at the University of Cambridge. Full details are provided in the main manuscript text and table footnotes.

The auxiliary material comprises Tables S1-S6:

**Table S1: Radiocarbon data for SK129-CR2**

**Table S2: Age model tie points for SK129-CR2**

**Table S3: Stable oxygen and carbon isotope data from SK129-CR2**

**Table S4: Neodymium isotope data from sediment leachates in SK129-CR2**

**Table S5: Neodymium isotope data from uncleaned foraminifera and fish teeth in SK129-CR2**

**Table S6: Composite neodymium isotope record from SK129-CR2, including data from decarbonated leachates, non-decarbonated leachates, uncleaned foraminifera and fish teeth.**

**Table S1:** Radiocarbon data for SK129-CR2.

| Depth (cm) | Sample identification | Species | $^{14}$C age (yrs) | error | $^{14}$C age res. corr. (yrs) | Calendar age (yrs BP) | error |
|---|---|---|---|---|---|---|---|
| 2.5 | SUERC-13140 | *sacculifer* | 3727 | 35 | 3377 | 3616 | 43 |
| 12 | SUERC-13141 | *sacculifer* | 6039 | 35 | 5689 | 6462 | 39 |
| 18 | SUERC-13142 | *sacculifer* | 9170 | 35 | 8820 | 9876 | 107 |
| 22 | SUERC-13143 | *sacculifer* | 9038 | 35 | 8688 | 9618 | 50 |
| 26 | SUERC-13144 | *sacculifer* | 11896 | 38 | 11546 | 13411 | 59 |
| 30 | SUERC-13147 | *sacculifer* | 13048 | 39 | 12698 | 14796 | 88 |
| 36 | SUERC-13148 | *sacculifer* | 14341 | 43 | 13991 | 16320 | 126 |
| 40 | SUERC-13149 | *sacculifer* | 14117 | 42 | 13767 | 16026 | 118 |
| 44 | SUERC-13150 | *sacculifer* | 14909 | 44 | 14559 | 17249 | 171 |
| 52 | SUERC-13665 | *sacculifer* | 17841 | 61 | 17491 | 20677 | 102 |
| 58 | ANU-5020* | *menardii* | 21580 | 80 | 21230 | 25421 | 129 |
| 64 | SUERC-13669 | *sacculifer* | 22409 | 94 | 22059 | 26536 | 147 |
| 78 | SUERC-13671 | *ruber* | 28849 | 189 | 28499 | 33888 | 248 |

***Notes:***
Radiocarbon analysis of planktonic foraminifera at the Scottish Universities Environmental Research Centre (SUERC) AMS Facility (5MV NEC AMS), except for sample at 58cm (denoted by *) which was picked by Luke Skinner and run by Stewart Fallon at the Australian National University AMS Lab. SUERC analyses were funded by grant allocation 1198.1006. Samples were hydrolysed to $CO_2$ using 85% orthophosphoric acid at 25°C. The gas was converted to graphite by Fe/Zn reduction. The errors are reported as 1σ. Conversion applied a uniform 350 y reservoir correction [*Butzin et al.*, 2005; *Cao et al.*, 2007] and was converted to calendar years using the *Fairbanks et al.* [2005] calibration curve 01.07 (see http://radiocarbon.LDEO.columbia.edu). This data corrects that presented in *Piotrowski et al.* [2009] which had an error in how the reservoir correction was applied.

**Table S2**: Age model tie points for SK129-CR2.

| Depth (cm) | Calendar age (ka BP) | Sed rate below (cm/ka) | Method | Notes |
|---|---|---|---|---|
| 2.5 | 3.616 | 3.34 | $^{14}C$ | |
| 12 | 6.462 | 2.44 | $^{14}C$ | |
| 20 | 9.747 | 1.64 | $^{14}C$ ave | average of two closely spaced $^{14}C$ measurements |
| 26 | 13.411 | 2.89 | $^{14}C$ | |
| 30 | 14.796 | 5.81 | $^{14}C$ | |
| 38 | 16.173 | 5.58 | $^{14}C$ ave | average of two closely spaced $^{14}C$ measurements |
| 44 | 17.249 | 2.33 | $^{14}C$ | |
| 52 | 20.677 | 1.26 | $^{14}C$ | |
| 58 | 25.421 | 5.38 | $^{14}C$ | |
| 64 | 26.536 | 1.90 | $^{14}C$ | |
| 78 | 33.888 | 1.99 | $^{14}C$ | |
| 156 | 73 | 2.00 | MIS 4/5 | |
| 160 | 75 | 1.72 | YTT | first appearance of Youngest Toba Tuff |
| 258 | 132 | 2.41 | MIS 5/6 | |
| 400 | 191 | 1.41 | MIS 6/7 | |
| 438 | 218 | 2.80 | MIS 7.3/7.4 | |
| 480 | 233 | 1.67 | MIS 7.4/7.5 | |
| 500 | 245 | 2.80 | MIS 7/8 | sedimentation rate below MIS 7-8 boundary is unconstrained and based on sedimentation rate in the subsequent glacial period MIS 7.4 |

***Notes:***
The age model is constrained by radiocarbon dates for 0-34 ka, and thereafter graphical correlation of benthic $\delta^{18}O$ to the LR04 benthic $\delta^{18}O$ stack [*Lisiecki and Raymo*, 2005]. The first appearance of the Youngest Toba Tuff [*Banakar*, 2005; *Mark et al.*, 2014] also provides an independent age estimate that is consistent with the LR04 based age model.

**Table S3:** Stable oxygen and carbon isotope data from SK129-CR2.

| Depth (cm) | Age (ka BP) | $\delta^{18}O_{Cib}$ EPSL | $\delta^{13}C_{Cib}$ EPSL | $\delta^{18}O_{Cib}$ this study | $\delta^{13}C_{Cib}$ this study | $\delta^{18}O_{Cib}$ combined | $\delta^{13}C_{Cib}$ combined |
|---|---|---|---|---|---|---|---|
| 0 | 2.28 | 2.88 | 0.53 | | | **2.88** | **0.53** |
| 8 | 5.26 | 2.55 | 0.47 | | | **2.55** | **0.47** |
| 14 | 7.28 | 2.72 | 0.44 | | | **2.72** | **0.44** |
| 16 | 8.10 | 3.31 | -0.06 | | | **3.31** | **-0.06** |
| 18 | 8.93 | 3.41 | 0.23 | | | **3.41** | **0.23** |
| 22 | 10.97 | 3.84 | 0.12 | | | **3.84** | **0.12** |
| 24 | 12.19 | 4.01 | 0.00 | | | **4.01** | **0.00** |
| 26 | 13.41 | 4.16 | 0.00 | | | **4.16** | **0.00** |
| 30 | 14.80 | 4.14 | 0.03 | | | **4.14** | **0.03** |
| 32 | 15.14 | 4.04 | -0.07 | | | **4.04** | **-0.07** |
| 36 | 15.83 | 4.53 | -0.09 | | | **4.53** | **-0.09** |
| 40 | 16.53 | 4.15 | -0.24 | | | **4.15** | **-0.24** |
| 44 | 17.25 | 4.16 | -0.18 | | | **4.16** | **-0.18** |
| 48 | 18.96 | 4.22 | -0.10 | | | **4.22** | **-0.10** |
| 52 | 20.68 | 4.13 | -0.14 | | | **4.13** | **-0.14** |
| 56 | 23.84 | 4.20 | -0.11 | | | **4.20** | **-0.11** |
| 58 | 25.42 | 4.12 | -0.15 | | | **4.12** | **-0.15** |
| 60 | 25.79 | 3.96 | -0.06 | | | **3.96** | **-0.06** |
| 62 | 26.16 | 4.10 | -0.09 | | | **4.10** | **-0.09** |
| 64 | 26.54 | 4.01 | -0.21 | | | **4.01** | **-0.21** |
| 66 | 27.59 | 4.22 | -0.08 | | | **4.22** | **-0.08** |
| 68 | 28.64 | 4.24 | -0.01 | | | **4.24** | **-0.01** |
| 70 | 29.69 | 3.62 | 0.10 | | | **3.62** | **0.10** |
| 72 | 30.74 | 3.79 | -0.10 | | | **3.79** | **-0.10** |
| 74 | 31.79 | 3.77 | 0.11 | | | **3.77** | **0.11** |
| 76 | 32.84 | 3.88 | 0.04 | | | **3.88** | **0.04** |
| 78 | 33.89 | 3.76 | 0.05 | | | **3.76** | **0.05** |
| 80 | 34.89 | 3.78 | 0.13 | | | **3.78** | **0.13** |
| 82 | 35.89 | 3.77 | 0.04 | | | **3.77** | **0.04** |
| 84 | 36.90 | 3.81 | 0.02 | | | **3.81** | **0.02** |
| 86 | 37.90 | 3.93 | 0.04 | | | **3.93** | **0.04** |
| 88 | 38.90 | 3.90 | 0.05 | | | **3.90** | **0.05** |
| 90 | 39.91 | 3.81 | 0.08 | | | **3.81** | **0.08** |
| 92 | 40.91 | 3.93 | 0.15 | | | **3.93** | **0.15** |
| 94 | 41.91 | 3.84 | 0.13 | | | **3.84** | **0.13** |
| 96 | 42.91 | 3.89 | -0.12 | | | **3.89** | **-0.12** |
| 98 | 43.92 | 3.53 | 0.20 | | | **3.53** | **0.20** |
| 100 | 44.92 | 3.65 | 0.07 | | | **3.65** | **0.07** |
| 102 | 45.92 | 3.69 | 0.03 | | | **3.69** | **0.03** |
| 104 | 46.93 | 3.67 | 0.06 | | | **3.67** | **0.06** |
| 106 | 47.93 | 3.59 | -0.05 | | | **3.59** | **-0.05** |
| 108 | 48.93 | 3.68 | 0.09 | | | **3.68** | **0.09** |
| 110 | 49.93 | 3.76 | 0.02 | | | **3.76** | **0.02** |
| 112 | 50.94 | 3.73 | 0.01 | | | **3.73** | **0.01** |
| 114 | 51.94 | 3.66 | -0.08 | | | **3.66** | **-0.08** |
| 116 | 52.94 | 3.80 | 0.13 | | | **3.80** | **0.13** |
| 118 | 53.95 | 3.60 | 0.02 | | | **3.60** | **0.02** |
| 120 | 54.95 | 3.63 | -0.02 | | | **3.63** | **-0.02** |

| | | | | | | | |
|---|---|---|---|---|---|---|---|
| 124 | 56.95 | 3.59 | -0.10 | | | **3.59** | **-0.10** |
| 132 | 60.97 | 3.71 | -0.21 | | | **3.71** | **-0.21** |
| 140 | 64.98 | 3.94 | -0.16 | | | **3.94** | **-0.16** |
| 142 | 65.98 | 4.09 | 0.04 | | | **4.09** | **0.04** |
| 144 | 66.98 | 4.36 | -0.05 | | | **4.36** | **-0.05** |
| 146 | 67.99 | 3.98 | -0.17 | | | **3.98** | **-0.17** |
| 148 | 68.99 | 4.18 | -0.05 | | | **4.18** | **-0.05** |
| 150 | 69.99 | 3.77 | -0.10 | | | **3.77** | **-0.10** |
| 152 | 70.99 | 3.87 | -0.01 | | | **3.87** | **-0.01** |
| 154 | 72.00 | 3.85 | 0.02 | | | **3.85** | **0.02** |
| 156 | 73.00 | 3.57 | 0.11 | | | **3.57** | **0.11** |
| 160 | 75.00 | 3.38 | 0.13 | | | **3.38** | **0.13** |
| 162 | 76.16 | 4.07 | 0.44 | | | **4.07** | **0.44** |
| 164 | 77.33 | 3.53 | 0.23 | | | **3.53** | **0.23** |
| 166 | 78.49 | 3.28 | 0.09 | | | **3.28** | **0.09** |
| 168 | 79.65 | 3.21 | 0.18 | | | **3.21** | **0.18** |
| 170 | 80.82 | 3.21 | 0.19 | | | **3.21** | **0.19** |
| 172 | 81.98 | 3.41 | 0.32 | | | **3.41** | **0.32** |
| 174 | 83.14 | 3.32 | 0.41 | | | **3.32** | **0.41** |
| 178 | 85.47 | | | 3.33 | 0.31 | **3.33** | **0.31** |
| 186 | 90.12 | 3.42 | 0.07 | | | **3.42** | **0.07** |
| 194 | 94.78 | 3.12 | 0.13 | | | **3.12** | **0.13** |
| 198 | 97.10 | | | 3.21 | 0.03 | **3.21** | **0.03** |
| 210 | 104.08 | 3.15 | 0.11 | | | **3.15** | **0.11** |
| 214 | 106.41 | 3.31 | 0.07 | | | **3.31** | **0.07** |
| 218 | 108.73 | 3.29 | 0.07 | | | **3.29** | **0.07** |
| 222 | 111.06 | 3.45 | 0.30 | | | **3.45** | **0.30** |
| 224 | 112.22 | 3.33 | 0.03 | | | **3.33** | **0.03** |
| 228 | 114.55 | 2.85 | -0.08 | | | **2.85** | **-0.08** |
| 232 | 116.88 | 3.08 | -0.12 | | | **3.08** | **-0.12** |
| 236 | 119.20 | 3.18 | 0.06 | | | **3.18** | **0.06** |
| 240 | 121.53 | 2.88 | -0.04 | | | **2.88** | **-0.04** |
| 242 | 122.69 | 2.71 | 0.13 | | | **2.71** | **0.13** |
| 244 | 123.86 | 2.88 | 0.00 | | | **2.88** | **0.00** |
| 248 | 126.18 | 3.34 | 0.19 | | | **3.34** | **0.19** |
| 250 | 127.35 | 2.70 | 0.07 | | | **2.70** | **0.07** |
| 252 | 128.51 | 2.86 | 0.20 | | | **2.86** | **0.20** |
| 254 | 129.67 | 2.21 | -0.21 | | | **2.21** | **-0.21** |
| 256 | 130.84 | 3.44 | 0.03 | | | **3.44** | **0.03** |
| 258 | 132.00 | 2.44 | -0.18 | | | **2.44** | **-0.18** |
| 260 | 132.83 | 3.89 | -0.32 | | | **3.89** | **-0.32** |
| 262 | 133.66 | 4.21 | -0.31 | | | **4.21** | **-0.31** |
| 264 | 134.49 | 4.01 | -0.24 | | | **4.01** | **-0.24** |
| 266 | 135.32 | 4.18 | -0.39 | | | **4.18** | **-0.39** |
| 270 | 136.99 | 4.13 | -0.32 | | | **4.13** | **-0.32** |
| 274 | 138.65 | 4.40 | -0.46 | | | **4.40** | **-0.46** |
| 278 | 140.31 | 4.27 | -0.37 | | | **4.27** | **-0.37** |
| 282 | 141.97 | 4.14 | -0.42 | | | **4.14** | **-0.42** |
| 286 | 143.63 | 4.30 | -0.40 | | | **4.30** | **-0.40** |
| 290 | 145.30 | 4.19 | -0.39 | | | **4.19** | **-0.39** |
| 294 | 146.96 | 4.11 | -0.31 | | | **4.11** | **-0.31** |
| 298 | 148.62 | 4.15 | -0.41 | | | **4.15** | **-0.41** |

| | | | | | | | |
|---|---|---|---|---|---|---|---|
| 300 | 149.45 | 4.17 | -0.40 | | | **4.17** | **-0.40** |
| 306 | 151.94 | 4.33 | -0.16 | | | **4.33** | **-0.16** |
| 320 | 157.76 | | | 4.13 | -0.43 | **4.13** | **-0.43** |
| 326 | 160.25 | | | 4.09 | -0.27 | **4.09** | **-0.27** |
| 334 | 163.58 | | | 3.75 | -0.38 | **3.75** | **-0.38** |
| 342 | 166.90 | | | 4.11 | -0.32 | **4.11** | **-0.32** |
| 344 | 167.73 | | | 3.78 | -0.28 | **3.78** | **-0.28** |
| 344 | 167.73 | | | 3.95 | -0.42 | **3.95** | **-0.42** |
| 346 | 168.56 | | | 3.80 | -0.22 | **3.80** | **-0.22** |
| 350 | 170.23 | | | 3.77 | -0.22 | **3.77** | **-0.22** |
| 352 | 171.06 | | | 3.79 | -0.20 | **3.79** | **-0.20** |
| 356 | 172.72 | | | 3.78 | -0.25 | **3.78** | **-0.25** |
| 358 | 173.55 | | | 3.84 | -0.49 | **3.84** | **-0.49** |
| 364 | 176.04 | | | 3.89 | -0.10 | **3.89** | **-0.10** |
| 366 | 176.87 | | | 3.89 | -0.32 | **3.89** | **-0.32** |
| 374 | 180.20 | | | 3.97 | -0.20 | **3.97** | **-0.20** |
| 378 | 181.86 | | | 3.82 | -0.31 | **3.82** | **-0.31** |
| 380 | 182.69 | | | 3.63 | -0.39 | **3.63** | **-0.39** |
| 382 | 183.52 | | | 3.97 | -0.45 | **3.97** | **-0.45** |
| 384 | 184.35 | | | 3.86 | -0.42 | **3.86** | **-0.42** |
| 386 | 185.18 | | | 3.91 | -0.59 | **3.91** | **-0.59** |
| 390 | 186.85 | | | 3.91 | -0.62 | **3.91** | **-0.62** |
| 392 | 187.68 | | | 3.71 | -0.35 | **3.71** | **-0.35** |
| 394 | 188.51 | | | 3.84 | -0.43 | **3.84** | **-0.43** |
| 396 | 189.34 | | | 3.44 | -0.20 | **3.44** | **-0.20** |
| 400 | 191.00 | | | 3.55 | -0.34 | **3.55** | **-0.34** |
| 402 | 192.42 | | | 3.21 | -0.16 | **3.21** | **-0.16** |
| 402 | 192.42 | | | 3.31 | -0.45 | **3.31** | **-0.45** |
| 404 | 193.84 | | | 3.42 | -0.09 | **3.42** | **-0.09** |
| 408 | 196.68 | | | 3.28 | -0.04 | **3.28** | **-0.04** |
| 410 | 198.11 | | | 3.60 | -0.23 | **3.60** | **-0.23** |
| 412 | 199.53 | | | 3.20 | 0.17 | **3.20** | **0.17** |
| 414 | 200.95 | | | 3.18 | 0.21 | **3.18** | **0.21** |
| 416 | 202.37 | | | 3.10 | 0.15 | **3.10** | **0.15** |
| 418 | 203.79 | | | 3.00 | 0.12 | **3.00** | **0.12** |
| 420 | 205.21 | | | 3.06 | 0.15 | **3.06** | **0.15** |
| 422 | 206.63 | | | 3.33 | 0.16 | **3.33** | **0.16** |
| 424 | 208.05 | | | 3.31 | -0.01 | **3.31** | **-0.01** |
| 426 | 209.47 | | | 3.17 | 0.12 | **3.17** | **0.12** |
| 426 | 209.47 | | | 3.49 | 0.22 | **3.49** | **0.22** |
| 428 | 210.89 | | | 3.21 | 0.10 | **3.21** | **0.10** |
| 432 | 213.74 | | | 2.97 | 0.09 | **2.97** | **0.09** |
| 438 | 218.00 | | | 3.18 | 0.29 | **3.18** | **0.29** |
| 444 | 220.14 | | | 3.67 | -0.15 | **3.67** | **-0.15** |
| 446 | 220.86 | | | 2.93 | -0.07 | **2.93** | **-0.07** |
| 450 | 222.29 | | | 3.61 | -0.26 | **3.61** | **-0.26** |
| 456 | 224.43 | | | 3.57 | -0.07 | **3.57** | **-0.07** |
| 462 | 226.57 | | | 3.48 | 0.03 | **3.48** | **0.03** |
| 468 | 228.71 | | | 3.62 | -0.20 | **3.62** | **-0.20** |
| 474 | 230.86 | | | 3.61 | -0.24 | **3.61** | **-0.24** |
| 480 | 233.00 | | | 3.40 | -0.03 | **3.40** | **-0.03** |
| 484 | 235.40 | | | 3.38 | 0.37 | **3.38** | **0.37** |

| | | | | | | | |
|---|---|---|---|---|---|---|---|
| 488 | 237.80 | | | 3.11 | 0.12 | **3.11** | **0.12** |
| 490 | 239.00 | | | 3.20 | 0.04 | **3.20** | **0.04** |
| 490 | 239.00 | | | 3.28 | 0.20 | **3.28** | **0.20** |
| 494 | 241.40 | | | 2.78 | 0.18 | **2.78** | **0.18** |
| 498 | 243.80 | | | 3.06 | 0.09 | **3.06** | **0.09** |
| 500 | 245.00 | | | 3.70 | -0.32 | **3.70** | **-0.32** |
| 504 | 246.43 | | | 3.90 | -0.25 | **3.90** | **-0.25** |
| 508 | 247.86 | | | 3.88 | -0.14 | **3.88** | **-0.14** |
| 512 | 249.29 | | | 3.88 | -0.32 | **3.88** | **-0.32** |
| 518 | 251.43 | | | 3.88 | -0.31 | **3.88** | **-0.31** |

***Notes:***
Data from *Piotrowski et al.* [2009] (referred to as 'EPSL') and this study. All data from *C. wuellerstorfi*.

**Table S4:** Neodymium isotope data from sediment leachates in SK129-CR2.

| Depth (cm) | Age (ka BP) | Notes | $\varepsilon_{Nd}$ decarbonated leachate | 2σ | Ref | Size (g) | Number of acetic acid leaches | $\varepsilon_{Nd}$ corrected | 2σ | Correction magnitude | Correction method | $\varepsilon_{Nd}$ non-decarbonated leachate | 2σ | Size (g) | Number of acetic acid leaches | $\varepsilon_{Nd}$ combined leachates | 2σ |
|---|---|---|---|---|---|---|---|---|---|---|---|---|---|---|---|---|---|
| 2.5 | 3.62 | | -9.60 | 0.20 | EPSL | | | -9.90 | 0.36 | -0.30 | constant | | | | | **-9.90** | **0.36** |
| 6 | 4.66 | | -9.90 | 0.32 | EPSL | | | -10.20 | 0.44 | -0.30 | constant | | | | | **-10.20** | **0.44** |
| 10 | 5.86 | | -9.28 | 0.24 | EPSL | | | -9.58 | 0.38 | -0.30 | constant | | | | | **-9.58** | **0.38** |
| 14 | 7.28 | | -8.82 | 0.20 | EPSL | | | -9.12 | 0.36 | -0.30 | constant | | | | | **-9.12** | **0.36** |
| 18 | 8.93 | | -8.51 | 0.36 | EPSL | | | -8.81 | 0.47 | -0.30 | constant | | | | | **-8.81** | **0.47** |
| 18 | 8.93 | | -8.45 | 0.24 | EPSL | | | -8.75 | 0.38 | -0.30 | constant | | | | | **-8.75** | **0.38** |
| 22 | 10.97 | | -8.52 | 0.20 | EPSL | | | -8.82 | 0.36 | -0.30 | constant | | | | | **-8.82** | **0.36** |
| 26 | 13.41 | | -7.41 | 0.24 | EPSL | | | -7.71 | 0.38 | -0.30 | constant | | | | | **-7.71** | **0.38** |
| 30 | 14.80 | | -7.39 | 0.19 | EPSL | | | -7.69 | 0.36 | -0.30 | constant | | | | | **-7.69** | **0.36** |
| 38 | 16.17 | | -6.85 | 0.19 | EPSL | | | -7.15 | 0.36 | -0.30 | constant | | | | | **-7.15** | **0.36** |
| 44 | 17.25 | | -6.76 | 0.21 | EPSL | | | -7.06 | 0.37 | -0.30 | constant | | | | | **-7.06** | **0.37** |
| 44 | 17.25 | | -6.66 | 0.24 | EPSL | | | -6.96 | 0.38 | -0.30 | constant | | | | | **-6.96** | **0.38** |
| 52 | 20.68 | | -6.31 | 0.24 | EPSL | | | -6.61 | 0.38 | -0.30 | constant | | | | | **-6.61** | **0.38** |
| 52 | 20.68 | | -6.31 | 0.24 | EPSL | | | -6.61 | 0.38 | -0.30 | constant | | | | | **-6.61** | **0.38** |
| 56 | 23.84 | | -6.93 | 0.21 | EPSL | | | -7.23 | 0.37 | -0.30 | constant | | | | | **-7.23** | **0.37** |
| 58 | 25.42 | | -6.38 | 0.25 | EPSL | | | -6.68 | 0.39 | -0.30 | constant | | | | | **-6.68** | **0.39** |
| 60 | 25.79 | | -6.52 | 0.24 | EPSL | | | -6.82 | 0.38 | -0.30 | constant | | | | | **-6.82** | **0.38** |
| 62 | 26.16 | | -6.92 | 0.25 | EPSL | | | -7.22 | 0.39 | -0.30 | constant | | | | | **-7.22** | **0.39** |
| 64 | 26.54 | | -7.48 | 0.20 | EPSL | | | -7.78 | 0.36 | -0.30 | constant | | | | | **-7.78** | **0.36** |
| 66 | 27.59 | | -6.63 | 0.25 | EPSL | | | -6.93 | 0.39 | -0.30 | constant | | | | | **-6.93** | **0.39** |
| 68 | 28.64 | | -6.66 | 0.25 | EPSL | | | -6.96 | 0.39 | -0.30 | constant | | | | | **-6.96** | **0.39** |
| 70 | 29.69 | | -7.75 | 0.22 | EPSL | | | -8.05 | 0.37 | -0.30 | constant | | | | | **-8.05** | **0.37** |
| 74 | 31.79 | | -7.46 | 0.20 | EPSL | | | -7.76 | 0.36 | -0.30 | constant | | | | | **-7.76** | **0.36** |
| 76 | 32.84 | | -6.96 | 0.25 | EPSL | | | -7.26 | 0.39 | -0.30 | constant | | | | | **-7.26** | **0.39** |
| 78 | 33.89 | | -7.24 | 0.25 | EPSL | | | -7.54 | 0.39 | -0.30 | constant | | | | | **-7.54** | **0.39** |

| | | | | | | | | | | | | | | | | | |
|---|---|---|---|---|---|---|---|---|---|---|---|---|---|---|---|---|---|
| 78 | 33.89 | | -6.30 | 0.25 | EPSL | | | -6.60 | 0.39 | -0.30 | constant | | | | | **-6.60** | **0.39** |
| 80 | 34.89 | | -7.09 | 0.25 | EPSL | | | -7.39 | 0.39 | -0.30 | constant | | | | | **-7.39** | **0.39** |
| 82 | 35.89 | | -7.05 | 0.24 | EPSL | | | -7.35 | 0.38 | -0.30 | constant | | | | | **-7.35** | **0.38** |
| 86 | 37.90 | | -7.76 | 0.20 | EPSL | | | -8.06 | 0.36 | -0.30 | constant | | | | | **-8.06** | **0.36** |
| 90 | 39.91 | | -7.37 | 0.21 | EPSL | | | -7.67 | 0.37 | -0.30 | constant | | | | | **-7.67** | **0.37** |
| 92 | 40.91 | | -7.00 | 0.25 | EPSL | | | -7.30 | 0.39 | -0.30 | constant | | | | | **-7.30** | **0.39** |
| 94 | 41.91 | | -7.13 | 0.25 | EPSL | | | -7.43 | 0.39 | -0.30 | constant | | | | | **-7.43** | **0.39** |
| 96 | 42.91 | | -7.29 | 0.20 | EPSL | | | -7.59 | 0.36 | -0.30 | constant | | | | | **-7.59** | **0.36** |
| 98 | 43.92 | | -6.98 | 0.25 | EPSL | | | -7.28 | 0.39 | -0.30 | constant | | | | | **-7.28** | **0.39** |
| 100 | 44.92 | | -6.76 | 0.25 | EPSL | | | -7.06 | 0.39 | -0.30 | constant | | | | | **-7.06** | **0.39** |
| 102 | 45.92 | | -7.06 | 0.24 | EPSL | | | -7.36 | 0.38 | -0.30 | constant | | | | | **-7.36** | **0.38** |
| 104 | 46.93 | | -7.32 | 0.25 | EPSL | | | -7.62 | 0.39 | -0.30 | constant | | | | | **-7.62** | **0.39** |
| 106 | 47.93 | | -7.79 | 0.20 | EPSL | | | -8.09 | 0.36 | -0.30 | constant | | | | | **-8.09** | **0.36** |
| 108 | 48.93 | | -7.80 | 0.25 | EPSL | | | -8.10 | 0.39 | -0.30 | constant | | | | | **-8.10** | **0.39** |
| 110 | 49.93 | | -8.22 | 0.23 | EPSL | | | -8.52 | 0.38 | -0.30 | constant | | | | | **-8.52** | **0.38** |
| 112 | 50.94 | | -7.57 | 0.25 | EPSL | | | -7.87 | 0.39 | -0.30 | constant | | | | | **-7.87** | **0.39** |
| 114 | 51.94 | | -8.00 | 0.20 | EPSL | | | -8.30 | 0.36 | -0.30 | constant | | | | | **-8.30** | **0.36** |
| 116 | 52.94 | | -6.90 | 0.36 | EPSL | | | -7.20 | 0.47 | -0.30 | constant | | | | | **-7.20** | **0.47** |
| 118 | 53.95 | | -7.36 | 0.25 | EPSL | | | -7.66 | 0.39 | -0.30 | constant | | | | | **-7.66** | **0.39** |
| 124 | 56.95 | | -7.37 | 0.24 | EPSL | | | -7.67 | 0.38 | -0.30 | constant | | | | | **-7.67** | **0.38** |
| 132 | 60.97 | | -7.59 | 0.21 | EPSL | | | -7.89 | 0.37 | -0.30 | constant | | | | | **-7.89** | **0.37** |
| 140 | 64.98 | | -7.62 | 0.18 | EPSL | | | -7.92 | 0.35 | -0.30 | constant | | | | | **-7.92** | **0.35** |
| 148 | 68.99 | | -7.28 | 0.24 | EPSL | | | -7.58 | 0.38 | -0.30 | constant | | | | | **-7.58** | **0.38** |
| 152 | 70.99 | | -8.36 | 0.18 | EPSL | | | -8.66 | 0.35 | -0.30 | constant | | | | | **-8.66** | **0.35** |
| 158 | 74.00 | | -8.20 | 0.22 | EPSL | | | -8.50 | 0.37 | -0.30 | constant | | | | | **-8.50** | **0.37** |
| 162 | 76.16 | | -9.02 | 0.18 | EPSL | | | -9.32 | 0.35 | -0.30 | constant | | | | | **-9.32** | **0.35** |
| 174 | 83.14 | | -9.09 | 0.18 | EPSL | | | -9.39 | 0.35 | -0.30 | constant | | | | | **-9.39** | **0.35** |
| 186 | 90.12 | | -8.96 | 0.20 | EPSL | | | -9.26 | 0.36 | -0.30 | constant | | | | | **-9.26** | **0.36** |
| 194 | 94.78 | | -9.05 | 0.20 | EPSL | | | -9.35 | 0.36 | -0.30 | constant | | | | | **-9.35** | **0.36** |
| 210 | 104.08 | | -9.21 | 0.24 | EPSL | | | -9.51 | 0.38 | -0.30 | constant | | | | | **-9.51** | **0.38** |

| | | | | | | | | | | | | | | | | | |
|---|---|---|---|---|---|---|---|---|---|---|---|---|---|---|---|---|---|
| 210 | 104.08 | | -9.13 | 0.22 | EPSL | | | -9.43 | 0.37 | -0.30 | constant | | | | | **-9.43** | **0.37** |
| 214 | 106.41 | | -9.30 | 0.20 | EPSL | | | -9.60 | 0.36 | -0.30 | constant | | | | | **-9.60** | **0.36** |
| 218 | 108.73 | | -9.04 | 0.25 | EPSL | | | -9.34 | 0.39 | -0.30 | constant | | | | | **-9.34** | **0.39** |
| 222 | 111.06 | | -8.72 | 0.24 | EPSL | | | -9.02 | 0.38 | -0.30 | constant | | | | | **-9.02** | **0.38** |
| 228 | 114.55 | | -8.56 | 0.24 | EPSL | | | -8.86 | 0.38 | -0.30 | constant | | | | | **-8.86** | **0.38** |
| 232 | 116.88 | | -8.38 | 0.20 | EPSL | | | -8.68 | 0.36 | -0.30 | constant | | | | | **-8.68** | **0.36** |
| 236 | 119.20 | | -8.51 | 0.24 | EPSL | | | -8.81 | 0.38 | -0.30 | constant | | | | | **-8.81** | **0.38** |
| 240 | 121.53 | | -9.24 | 0.20 | EPSL | | | -9.54 | 0.36 | -0.30 | constant | | | | | **-9.54** | **0.36** |
| 240 | 121.53 | | -8.86 | 0.23 | EPSL | | | -9.16 | 0.38 | -0.30 | constant | | | | | **-9.16** | **0.38** |
| 244 | 123.86 | | -8.73 | 0.22 | EPSL | | | -9.03 | 0.37 | -0.30 | constant | | | | | **-9.03** | **0.37** |
| 244 | 123.86 | | -8.61 | 0.20 | EPSL | | | -8.91 | 0.36 | -0.30 | constant | | | | | **-8.91** | **0.36** |
| 246 | 125.02 | | -8.38 | 0.22 | EPSL | | | -8.68 | 0.37 | -0.30 | constant | | | | | **-8.68** | **0.37** |
| 250 | 127.35 | | -8.55 | 0.20 | EPSL | | | -8.85 | 0.36 | -0.30 | constant | | | | | **-8.85** | **0.36** |
| 252 | 128.51 | | -8.67 | 0.25 | EPSL | | | -8.97 | 0.39 | -0.30 | constant | | | | | **-8.97** | **0.39** |
| 254 | 129.67 | | -7.49 | 0.20 | EPSL | | | -7.79 | 0.36 | -0.30 | constant | | | | | **-7.79** | **0.36** |
| 256 | 130.84 | | -6.92 | 0.25 | EPSL | | | -7.22 | 0.39 | -0.30 | constant | | | | | **-7.22** | **0.39** |
| 258 | 132.00 | | -7.36 | 0.22 | EPSL | | | -7.66 | 0.37 | -0.30 | constant | | | | | **-7.66** | **0.37** |
| 260 | 132.83 | | -6.09 | 0.22 | EPSL | | | -6.39 | 0.37 | -0.30 | constant | | | | | **-6.39** | **0.37** |
| 264 | 134.49 | | -7.32 | 0.24 | EPSL | | | -7.62 | 0.38 | -0.30 | constant | | | | | **-7.62** | **0.38** |
| 266 | 135.32 | | -7.03 | 0.25 | EPSL | | | -7.33 | 0.39 | -0.30 | constant | | | | | **-7.33** | **0.39** |
| 278 | 140.31 | | -6.44 | 0.20 | EPSL | | | -6.74 | 0.36 | -0.30 | constant | | | | | **-6.74** | **0.36** |
| 282 | 141.97 | | -7.33 | 0.22 | EPSL | | | -7.63 | 0.37 | -0.30 | constant | | | | | **-7.63** | **0.37** |
| 286 | 143.63 | | -6.76 | 0.20 | EPSL | | | -7.06 | 0.36 | -0.30 | constant | | | | | **-7.06** | **0.36** |
| 290 | 145.30 | | -7.39 | 0.22 | EPSL | | | -7.69 | 0.37 | -0.30 | constant | | | | | **-7.69** | **0.37** |
| 296 | 147.79 | | | | | | | | | | | -7.83 | 0.23 | 1.99 | 3 | **-7.83** | **0.23** |
| 304 | 151.11 | | | | | | | | | | | -8.15 | 0.19 | 2.08 | 3 | **-8.15** | **0.19** |
| 306 | 151.94 | | -6.34 | 0.25 | EPSL | | | -6.64 | 0.39 | -0.30 | constant | | | | | **-6.64** | **0.39** |
| 310 | 153.61 | | | | | | | | | | | -6.83 | 0.25 | 2.84 | 3 | **-6.83** | **0.25** |
| 320 | 157.76 | | -6.57 | 0.29 | this | 3.80 | 9 | -7.29 | 0.47 | -0.72 | size | | | | | **-7.29** | **0.47** |
| 326 | 160.25 | | -6.66 | 0.23 | this | 3.60 | 10 | -7.44 | 0.43 | -0.78 | size | | | | | **-7.44** | **0.43** |

| | | | | | | | | | | | | | | | | | |
|---|---|---|---|---|---|---|---|---|---|---|---|---|---|---|---|---|---|
| 328 | 161.08 | large | -7.02 | 0.26 | this | 4.61 | 10 | -7.47 | 0.45 | -0.46 | size | | | | | **-7.47** | **0.45** |
| 328 | 161.08 | small | -5.87 | 0.26 | this | 1.87 | 10 | -7.20 | 0.45 | -1.33 | size | | | | | **-7.20** | **0.45** |
| 334 | 163.58 | | -6.98 | 0.29 | this | 3.40 | 9 | -7.82 | 0.47 | -0.85 | size | | | | | **-7.82** | **0.47** |
| 342 | 166.90 | | -7.22 | 0.23 | this | 2.30 | 10 | -8.42 | 0.43 | -1.20 | size | | | | | **-8.42** | **0.43** |
| 344 | 167.73 | | -7.81 | 0.26 | this | 2.99 | 10 | -8.78 | 0.45 | -0.98 | size | | | | | **-8.78** | **0.45** |
| 346 | 168.56 | | -7.57 | 0.18 | this | 2.70 | 9 | -8.64 | 0.41 | -1.07 | size | | | | | **-8.64** | **0.41** |
| 350 | 170.23 | | -7.87 | 0.26 | this | 2.67 | 10 | -8.94 | 0.45 | -1.07 | size | | | | | **-8.94** | **0.45** |
| 352 | 171.06 | | -8.04 | 0.24 | this | 2.60 | 9 | -9.15 | 0.44 | -1.11 | size | | | | | **-9.15** | **0.44** |
| 356 | 172.72 | | -7.79 | 0.18 | this | 2.40 | 9 | -8.96 | 0.41 | -1.17 | size | | | | | **-8.96** | **0.41** |
| 358 | 173.55 | | -8.07 | 0.26 | this | 3.24 | 10 | -8.98 | 0.45 | -0.91 | size | | | | | **-8.98** | **0.45** |
| 364 | 176.04 | | -7.47 | 0.24 | this | 1.60 | 9 | -8.90 | 0.44 | -1.43 | size | | | | | **-8.90** | **0.44** |
| 366 | 176.87 | | -8.62 | 0.29 | this | 2.70 | 9 | -9.70 | 0.47 | -1.07 | size | | | | | **-9.70** | **0.47** |
| 370 | 178.54 | | -8.71 | 0.23 | this | 2.10 | 10 | -9.97 | 0.43 | -1.27 | size | | | | | **-9.97** | **0.43** |
| 372 | 179.37 | | | | | | | | | | | -9.41 | 0.43 | 6.70 | 4 | **-9.41** | **0.43** |
| 374 | 180.20 | | -8.20 | 0.24 | this | 1.10 | 9 | -9.80 | 0.44 | -1.59 | size | | | | | **-9.80** | **0.44** |
| 378 | 181.86 | | -8.20 | 0.29 | this | 6.00 | 9 | -8.20 | 0.47 | 0.00 | size | | | | | **-8.20** | **0.47** |
| 382 | 183.52 | | -7.32 | 0.18 | this | 3.40 | 9 | -8.17 | 0.41 | -0.85 | size | | | | | **-8.17** | **0.41** |
| 386 | 185.18 | | -8.07 | 0.29 | this | 4.80 | 9 | -8.46 | 0.47 | -0.39 | size | | | | | **-8.46** | **0.47** |
| 394 | 188.51 | | -8.27 | 0.29 | this | 4.90 | 9 | -8.63 | 0.47 | -0.36 | size | | | | | **-8.63** | **0.47** |
| 400 | 191.00 | | -8.43 | 0.23 | this | 3.40 | 10 | -9.27 | 0.43 | -0.85 | size | | | | | **-9.27** | **0.43** |
| 404 | 193.84 | | -8.59 | 0.26 | this | 3.37 | 11 | -9.44 | 0.45 | -0.85 | size | | | | | **-9.44** | **0.45** |
| 408 | 196.68 | | | | | | | | | | | -9.45 | 0.19 | 7.00 | 4 | **-9.45** | **0.19** |
| 410 | 198.11 | | -8.79 | 0.18 | this | 2.90 | 9 | -9.80 | 0.41 | -1.01 | size | | | | | **-9.80** | **0.41** |
| 414 | 200.95 | | -9.36 | 0.26 | this | 3.69 | 11 | -10.10 | 0.45 | -0.75 | size | | | | | **-10.10** | **0.45** |
| 420 | 205.21 | | -8.24 | 0.21 | this | 2.90 | 10 | -9.24 | 0.43 | -1.01 | size | | | | | **-9.24** | **0.43** |
| 422 | 206.63 | | | | | | | | | | | -9.46 | 0.19 | 7.61 | 4 | **-9.46** | **0.19** |
| 424 | 208.05 | | -9.34 | 0.29 | this | 3.60 | 9 | -10.12 | 0.47 | -0.78 | size | | | | | **-10.12** | **0.47** |
| 426 | 209.47 | | -8.67 | 0.26 | this | 2.98 | 11 | -9.64 | 0.45 | -0.98 | size | | | | | **-9.64** | **0.45** |
| 428 | 210.89 | | -8.97 | 0.23 | this | 3.00 | 10 | -9.95 | 0.43 | -0.98 | size | | | | | **-9.95** | **0.43** |
| 434 | 215.16 | large | -9.59 | 0.26 | this | 2.95 | 11 | -10.56 | 0.45 | -0.97 | size | | | | | **-10.56** | **0.45** |

| | | | | | | | | | | | | | | | | | |
|---|---|---|---|---|---|---|---|---|---|---|---|---|---|---|---|---|---|
| 434 | 215.16 | small | -8.76 | 0.26 | this | 1.67 | 11 | -10.16 | 0.45 | -1.40 | size | | | | | **-10.16** | **0.45** |
| 438 | 218.00 | | | | | | | | | | | -9.49 | 0.19 | 5.33 | 4 | **-9.49** | **0.19** |
| 444 | 220.14 | | -8.89 | 0.23 | this | 4.50 | 10 | -9.38 | 0.43 | -0.49 | size | | | | | **-9.38** | **0.43** |
| 446 | 220.86 | | | | | | | | | | | -9.19 | 0.19 | 6.48 | 4 | **-9.19** | **0.19** |
| 450 | 222.29 | | -8.58 | 0.29 | this | 4.70 | 9 | -9.00 | 0.47 | -0.42 | size | | | | | **-9.00** | **0.47** |
| 456 | 224.43 | | -8.25 | 0.23 | this | 5.60 | 10 | -8.38 | 0.43 | -0.13 | size | | | | | **-8.38** | **0.43** |
| 462 | 226.57 | | | | | | | | | | | -8.67 | 0.19 | 5.47 | 4 | **-8.67** | **0.19** |
| 468 | 228.71 | | -8.03 | 0.29 | this | 4.20 | 9 | -8.61 | 0.47 | -0.59 | size | | | | | **-8.61** | **0.47** |
| 474 | 230.86 | | -7.58 | 0.26 | this | 2.48 | 11 | -8.72 | 0.45 | -1.14 | size | | | | | **-8.72** | **0.45** |
| 480 | 233.00 | | -8.73 | 0.23 | this | 3.30 | 10 | -9.61 | 0.43 | -0.88 | size | | | | | **-9.61** | **0.43** |
| 484 | 235.40 | | | | | | | | | | | -9.54 | 0.19 | 7.93 | 4 | **-9.54** | **0.19** |
| 488 | 237.80 | | -8.91 | 0.26 | this | 2.70 | 11 | -9.99 | 0.45 | -1.07 | size | | | | | **-9.99** | **0.45** |
| 494 | 241.40 | | | | | | | | | | | -9.53 | 0.19 | 3.01 | 4 | **-9.53** | **0.19** |
| 498 | 243.80 | | -8.51 | 0.26 | this | 2.71 | 11 | -9.58 | 0.45 | -1.07 | size | | | | | **-9.58** | **0.45** |
| 500 | 245.00 | | -8.30 | 0.23 | this | 3.30 | 10 | -9.18 | 0.43 | -0.88 | size | | | | | **-9.18** | **0.43** |
| 504 | 246.43 | | -7.90 | 0.26 | this | 3.18 | 11 | -8.81 | 0.45 | -0.91 | size | | | | | **-8.81** | **0.45** |
| 508 | 247.86 | | -6.60 | 0.29 | this | 1.80 | 9 | -7.97 | 0.47 | -1.37 | size | | | | | **-7.97** | **0.47** |
| 512 | 249.29 | | -7.59 | 0.26 | this | 3.89 | 11 | -8.28 | 0.45 | -0.68 | size | | | | | **-8.28** | **0.45** |
| 518 | 251.43 | | | | | | | | | | | -8.48 | 0.19 | 5.60 | 4 | **-8.48** | **0.19** |

***Notes:***
This table includes decarbonated leachates from *Piotrowski et al.* [2009] ('EPSL' in column 'Ref'), decarbonated leachates from this study ('this' in column 'Ref'), corrected decarbonated leachates and details of the correction, and non-decarbonated leachates. All Nd isotope measurements were standard corrected to a JNdi-1 $\varepsilon_{Nd}$ value of 0.512115 that is consistent with *Tanaka et al.* [2000]. In the 'Notes' column, 'small' and 'large' refer to the leaching sample size tests (see Figures 2 and 3). Sample sizes are wet weights after decarbonation.

**Table S5:** Neodymium isotope data from uncleaned foraminifera and fish teeth in SK129-CR2.

| Depth (cm) | Age (ka BP) | $\varepsilon_{Nd}$ uncleaned foraminifera | 2σ | $\varepsilon_{Nd}$ fish teeth | 2σ |
|---|---|---|---|---|---|
| 6 | 4.66 | -9.82 | 0.40 | | |
| 44 | 17.25 | -7.21 | 0.40 | | |
| 86 | 37.90 | -8.03 | 0.40 | | |
| 140 | 64.98 | -7.96 | 0.28 | | |
| 244 | 123.86 | -9.20 | 0.40 | | |
| 320 | 157.76 | -7.14 | 0.28 | -7.32 | 0.44 |
| 366 | 176.87 | -8.59 | 0.28 | -9.08 | 0.68 |
| 394 | 188.51 | | | -7.89 | 0.68 |
| 404 | 193.84 | | | -9.70 | 0.44 |
| 414 | 200.95 | | | -9.83 | 0.68 |
| 424 | 208.05 | -9.27 | 0.40 | | |
| 498 | 243.80 | | | -9.40 | 0.37 |
| 512 | 249.29 | -8.38 | 0.28 | | |

***Notes:***
All Nd isotope data is corrected to a JNdi-1 $\varepsilon_{Nd}$ value of 0.512115 that is consistent with *Tanaka et al.* [2000].

**Table S6:** Composite neodymium isotope record from SK129-CR2, including data from decarbonated leachates, non-decarbonated leachates, uncleaned foraminifera and fish teeth.

| Depth (cm) | Age (ka BP) | $\varepsilon_{Nd}$ composite | 2σ |
|---|---|---|---|
| 2.5 | 3.62 | -9.90 | 0.36 |
| 6 | 4.66 | -10.20 | 0.44 |
| 6 | 4.66 | -9.82 | 0.40 |
| 10 | 5.86 | -9.58 | 0.38 |
| 14 | 7.28 | -9.12 | 0.36 |
| 18 | 8.93 | -8.81 | 0.47 |
| 18 | 8.93 | -8.75 | 0.38 |
| 22 | 10.97 | -8.82 | 0.36 |
| 26 | 13.41 | -7.71 | 0.38 |
| 30 | 14.80 | -7.69 | 0.36 |
| 38 | 16.17 | -7.15 | 0.36 |
| 44 | 17.25 | -7.21 | 0.40 |
| 44 | 17.25 | -7.06 | 0.37 |
| 44 | 17.25 | -6.96 | 0.38 |
| 52 | 20.68 | -6.61 | 0.38 |
| 52 | 20.68 | -6.61 | 0.38 |
| 56 | 23.84 | -7.23 | 0.37 |
| 58 | 25.42 | -6.68 | 0.39 |
| 60 | 25.79 | -6.82 | 0.38 |
| 62 | 26.16 | -7.22 | 0.39 |
| 64 | 26.54 | -7.78 | 0.36 |
| 66 | 27.59 | -6.93 | 0.39 |
| 68 | 28.64 | -6.96 | 0.39 |
| 70 | 29.69 | -8.05 | 0.37 |
| 74 | 31.79 | -7.76 | 0.36 |
| 76 | 32.84 | -7.26 | 0.39 |
| 78 | 33.89 | -7.54 | 0.39 |
| 78 | 33.89 | -6.60 | 0.39 |
| 80 | 34.89 | -7.39 | 0.39 |
| 82 | 35.89 | -7.35 | 0.38 |
| 86 | 37.90 | -8.06 | 0.36 |
| 86 | 37.90 | -8.03 | 0.40 |
| 90 | 39.91 | -7.67 | 0.37 |
| 92 | 40.91 | -7.30 | 0.39 |
| 94 | 41.91 | -7.43 | 0.39 |
| 96 | 42.91 | -7.59 | 0.36 |
| 98 | 43.92 | -7.28 | 0.39 |
| 100 | 44.92 | -7.06 | 0.39 |
| 102 | 45.92 | -7.36 | 0.38 |
| 104 | 46.93 | -7.62 | 0.39 |
| 106 | 47.93 | -8.09 | 0.36 |
| 108 | 48.93 | -8.10 | 0.39 |
| 110 | 49.93 | -8.52 | 0.38 |
| 112 | 50.94 | -7.87 | 0.39 |
| 114 | 51.94 | -8.30 | 0.36 |
| 116 | 52.94 | -7.20 | 0.47 |
| 118 | 53.95 | -7.66 | 0.39 |
| 124 | 56.95 | -7.67 | 0.38 |
| 132 | 60.97 | -7.89 | 0.37 |
| 140 | 64.98 | -7.92 | 0.35 |
| 140 | 64.98 | -7.96 | 0.28 |
| 148 | 68.99 | -7.58 | 0.38 |
| 152 | 70.99 | -8.66 | 0.35 |
| 158 | 74.00 | -8.50 | 0.37 |
| 162 | 76.16 | -9.32 | 0.35 |
| 174 | 83.14 | -9.39 | 0.35 |
| 186 | 90.12 | -9.26 | 0.36 |
| 194 | 94.78 | -9.35 | 0.36 |
| 210 | 104.08 | -9.51 | 0.38 |
| 210 | 104.08 | -9.43 | 0.37 |
| 214 | 106.41 | -9.60 | 0.36 |
| 218 | 108.73 | -9.34 | 0.39 |
| 222 | 111.06 | -9.02 | 0.38 |
| 228 | 114.55 | -8.86 | 0.38 |
| 232 | 116.88 | -8.68 | 0.36 |
| 236 | 119.20 | -8.81 | 0.38 |
| 240 | 121.53 | -9.16 | 0.38 |
| 240 | 121.53 | -9.54 | 0.36 |
| 244 | 123.86 | -9.20 | 0.40 |
| 244 | 123.86 | -9.03 | 0.37 |
| 244 | 123.86 | -8.91 | 0.36 |
| 246 | 125.02 | -8.68 | 0.37 |
| 250 | 127.35 | -8.85 | 0.36 |
| 252 | 128.51 | -8.97 | 0.39 |
| 254 | 129.67 | -7.79 | 0.36 |
| 256 | 130.84 | -7.22 | 0.39 |
| 258 | 132.00 | -7.66 | 0.37 |
| 260 | 132.83 | -6.39 | 0.37 |
| 264 | 134.49 | -7.62 | 0.38 |
| 266 | 135.32 | -7.33 | 0.39 |
| 278 | 140.31 | -6.74 | 0.36 |
| 282 | 141.97 | -7.63 | 0.37 |
| 286 | 143.63 | -7.06 | 0.36 |
| 290 | 145.30 | -7.69 | 0.37 |
| 296 | 147.79 | -7.83 | 0.23 |
| 304 | 151.11 | -8.15 | 0.19 |
| 306 | 151.94 | -6.64 | 0.39 |
| 310 | 153.61 | -6.83 | 0.25 |

| Depth (cm) | Age (ka BP) | $\varepsilon_{Nd}$ composite | 2σ |
|---|---|---|---|
| 320 | 157.76 | -7.29 | 0.47 |
| 320 | 157.76 | -7.14 | 0.28 |
| 320 | 157.76 | -7.32 | 0.44 |
| 326 | 160.25 | -7.44 | 0.43 |
| 328 | 161.08 | -7.47 | 0.45 |
| 328 | 161.08 | -7.20 | 0.45 |
| 334 | 163.58 | -7.82 | 0.47 |
| 342 | 166.90 | -8.42 | 0.43 |
| 344 | 167.73 | -8.78 | 0.45 |
| 346 | 168.56 | -8.64 | 0.41 |
| 350 | 170.23 | -8.94 | 0.45 |
| 352 | 171.06 | -9.15 | 0.44 |
| 356 | 172.72 | -8.96 | 0.41 |
| 358 | 173.55 | -8.98 | 0.45 |
| 364 | 176.04 | -8.90 | 0.44 |
| 366 | 176.87 | -8.59 | 0.28 |
| 366 | 176.87 | -9.70 | 0.47 |
| 370 | 178.54 | -9.97 | 0.43 |
| 372 | 179.37 | -9.41 | 0.43 |
| 374 | 180.20 | -9.80 | 0.44 |
| 378 | 181.86 | -8.20 | 0.47 |
| 382 | 183.52 | -8.17 | 0.41 |
| 386 | 185.18 | -8.46 | 0.47 |
| 394 | 188.51 | -8.63 | 0.47 |
| 400 | 191.00 | -9.27 | 0.43 |
| 404 | 193.84 | -9.44 | 0.45 |
| 404 | 193.84 | -9.70 | 0.44 |
| 408 | 196.68 | -9.45 | 0.19 |
| 410 | 198.11 | -9.80 | 0.41 |
| 414 | 200.95 | -10.10 | 0.45 |
| 420 | 205.21 | -9.24 | 0.43 |
| 422 | 206.63 | -9.46 | 0.19 |
| 424 | 208.05 | -9.27 | 0.40 |
| 424 | 208.05 | -10.12 | 0.47 |
| 426 | 209.47 | -9.64 | 0.45 |
| 428 | 210.89 | -9.95 | 0.43 |
| 434 | 215.16 | -10.56 | 0.45 |
| 434 | 215.16 | -10.16 | 0.45 |
| 438 | 218.00 | -9.49 | 0.19 |
| 444 | 220.14 | -9.38 | 0.43 |
| 446 | 220.86 | -9.19 | 0.19 |
| 450 | 222.29 | -9.00 | 0.47 |
| 456 | 224.43 | -8.38 | 0.43 |
| 462 | 226.57 | -8.67 | 0.19 |
| 468 | 228.71 | -8.61 | 0.47 |
| 474 | 230.86 | -8.72 | 0.45 |
| 480 | 233.00 | -9.61 | 0.43 |
| 484 | 235.40 | -9.54 | 0.19 |
| 488 | 237.80 | -9.99 | 0.45 |
| 494 | 241.40 | -9.53 | 0.19 |
| 498 | 243.80 | -9.58 | 0.45 |
| 498 | 243.80 | -9.40 | 0.37 |
| 500 | 245.00 | -9.18 | 0.43 |
| 504 | 246.43 | -8.81 | 0.45 |
| 508 | 247.86 | -7.97 | 0.47 |
| 512 | 249.29 | -8.28 | 0.45 |
| 512 | 249.29 | -8.38 | 0.28 |
| 518 | 251.43 | -8.48 | 0.19 |

***Notes:***
This composite record includes data from decarbonated leachates, non-decarbonated leachates, uncleaned foraminifera and fish teeth. The decarbonated leachate data were corrected for sample size as described in the manuscript text and Table S4. Three fish teeth data with large analytical uncertainties (0.68) are not included. All Nd isotope data is corrected to a JNdi-1 $\varepsilon_{Nd}$ value of 0.512115 that is consistent with *Tanaka et al.* [2000].

**References in Supplementary Information**


Banakar, V. K. (2005), $\delta^{13}C$ depleted oceans before the Termination 2: More nutrient-rich deep-water formation or light-carbon transfer?, *Indian J. Mar. Sci.*, *34*(3), 249-258.

Butzin, M., M. Prange, and G. Lohmann (2005), Radiocarbon simulations for the glacial ocean: The effects of wind stress, Southern Ocean sea ice and Heinrich events, *Earth Planet. Sci. Lett.*, *235*(1-2), 45-61.

Cao, L., R. G. Fairbanks, R. A. Mortlock, and M. J. Risk (2007), Radiocarbon reservoir age of high latitude North Atlantic surface water during the last deglacial, *Quat. Sci. Rev.*, *26*(5-6), 732-742.

Fairbanks, R. G., R. A. Mortlock, T. C. Chiu, L. Cao, A. Kaplan, T. P. Guilderson, T. W. Fairbanks, A. L. Bloom, P. M. Grootes, and M. J. Nadeau (2005), Radiocarbon calibration curve spanning 0 to 50,000 years BP based on paired $^{230}Th/^{234}U/^{238}U$ and $^{14}C$ dates on pristine corals, *Quat. Sci. Rev.*, *24*(16-17), 1781-1796.

Lisiecki, L. E., and M. E. Raymo (2005), A Pliocene-Pleistocene stack of 57 globally distributed benthic $\delta^{18}O$ records, *Paleoceanography*, *20*(1), doi: 10.1029/2004pa001071.

Mark, D. F., M. Petraglia, V. C. Smith, L. E. Morgan, D. N. Barfod, B. S. Ellis, N. J. Pearce, J. N. Pal, and R. Korisettar (2014), A high-precision $^{40}Ar/^{39}Ar$ age for the Young Toba Tuff and dating of ultra-distal tephra: forcing of Quaternary climate and implications for hominin occupation of India, *Quaternary Geochronology*, *21*, 90-103.

Piotrowski, A. M., V. K. Banakar, A. E. Scrivner, H. Elderfield, A. Galy, and A. Dennis (2009), Indian Ocean circulation and productivity during the last glacial cycle, *Earth Planet. Sci. Lett.*, *285*(1-2), 179-189.

Tanaka, T., et al. (2000), JNdi-1: a neodymium isotopic reference in consistency with LaJolla neodymium, *Chemical Geology*, *168*(3-4), 279-281.